Master Thesis

submitted within the UNIGIS MSc programme
Interfaculty Department of Geoinformatics - Z_GIS
University of Salzburg

Detection of Cropland Abandonment in a Crisis Situation

An Approach using Google Earth Engine and Sentinel-2 Imagery for the Ongoing Conflict in Cabo Delgado, Mozambique

by

Dipl.-Geogr. Merle Pottharst
106942

A thesis submitted in partial fulfilment of the requirements of the degree of
Master of Science – MSc

Advisor:

Dr. Lorenz Wendt

Caputh, January 31st, 2024

SCIENCE PLEDGE

By my signature below, I certify that my thesis is entirely the result of my own work.

I have cited all sources I have used in my thesis and I have always indicated their origin.

Caputh, January, 31st, 2024

Merle Pottharst

ACKNOWLEDGEMENTS

This project would not have been possible without the support of so many people.

First of all, I would like to thank my supervisor Lorenz Wendt very much for his ongoing support and so many valuable tips and important advice. He helped make sense of many confusions. I also would like to express my gratitude to the UNIGIS team who was always there with help, advice, and encouragement, not only throughout the master thesis but also during the whole program. The UNIGIS program wouldn't be what it is without the amazing team behind it.

A big thank you also goes to Philippe Rufin who has given me many valuable insights into the specifics of Cabo Delgado and the difficult task of classifying satellite data in regions like that.

I am very grateful to my proofreaders for giving me plenty of great feedback and new ideas.

Finally, thanks to my family and friends who endured this long process with me, always offering support and love!

ABSTRACT

Cropland abandonment in conflict zones poses a critical challenge, as rural populations, when perceiving threats to their safety, often flee their homes, resulting in the abandonment of vital agricultural land and exacerbating food insecurity. Swift and targeted assistance is imperative in such scenarios; however, obtaining reliable information about the affected population is hindered by the conflict. This study explores the use of satellite imagery, particularly Sentinel-2 data available on Google Earth Engine, to automatically detect cropland abandonment in Cabo Delgado, Mozambique - a region significantly impacted by an insurgency targeting civilians. The underlying assumption is that the abandonment of agricultural fields serves as an indicator of population displacement and food insecurity.

The research employs a novel approach by integrating Google Earth Engine with geospatial tools such as ArcGIS Pro and QGIS for a supervised classification using the Random Forest algorithm. Training data is derived from overlaying existing land-cover datasets and refining them to areas with consistent land-cover across datasets. This innovative approach aims to automate and expedite the often time-consuming and resource-intensive process of obtaining training data.

Drawing inspiration from successful studies in classifying agriculture within highly fragmented small-scale landscapes, our methodology integrates advanced features into the Random Forest model. These features encompass original bands (Red, Green, Blue, NIR, and SWIR), six spectral indices, three texture values, and five auxiliary features. The goal is to optimize classification accuracy, particularly in challenging environments. The resulting land-cover maps for 2020, 2021, and 2022 are analysed for accuracy through confusion matrices and common parameters. The detection of cropland abandonment employs post-classification change detection, specifically bi-temporal change analysis of classified maps. The underlying assumption is that fields transitioning from cropland to a different category in consecutive years can be presumed as abandoned. To explore possible correlations between cropland abandonment and the continuing conflict, conflict events data from the ACLED Project is finally compared to change maps for a visual interpretation.

With achieving accuracies between 58% and 65% for the classified maps, with even lower values for challenging classes such as cropland, bareland, and grassland, the study faces difficulties in analysing land-cover changes and their links to conflict events. It is suspected that misclassifications may result from the unique approach to generating training data. Nevertheless, when based on highly accurate datasets, particularly for challenging classes, this automated method offers a rapid and potentially useful way to obtain reference data.

The findings underscore the need for further refinement in training data generation and acknowledgement of potential limitations when applying such methodologies in conflict-affected areas. The study suggests avenues for methodological refinement to further explore the connection between conflict, cropland abandonment, and food insecurity.

List of Abbreviations

ACLED	Armed Conflict Location and Event Data
AEZ	Agroecological Zone
BI	Bare Soil Index
CART	Classification And Regression Trees
CCI	Climate Change Initiative
CEMS	Copernicus Emergency Management Service
CVA	Change Vector Analysis
ESA	European Space Agency
ESRI	Environmental Systems Research Institute
EO	Earth Observation
EVI	Enhanced Vegetation Index
GCVI	Green Chlorophyll Vegetation Index
IDP	Internally Displaced Person
LC	Land-Cover
LULC	Land-Use / Land-Cover
NDVI	Normalized Difference Vegetation Index
NDMI	Normalized Difference Moisture Index
NICFI	Norway's International Climate and Forest Initiative
NIR	Near-Infrared
OBIA	Object-Based Image Analysis
PA	Producer's Accuracy
RF	Random Forest
RGB	Red Green Blue
ROI	Region of Interest
RS	Remote Sensing
S2	Sentinel-2
SAVI	Soil Adjusted Vegetation Index
SWIR	Short-Wave-Infrared
UA	User's Accuracy
ZRB	Zambezi River Basin

Contents

SCIENCE PLEDGE **I**

ACKNOWLEDGEMENTS **II**

ABSTRACT **III**

List of Abbreviations **IV**

1 Introduction **1**

2 Materials and Methods **8**

2.1 Study Area 9
2.2 Data 10
2.3 Pre-Processing 10
2.4 Training Data Generation 13
2.5 Classification 15
2.6 Accuracy Analysis and Validation 16
2.7 Change Detection 16
2.8 Overlay with Conflict Data 17

3 Results **19**

3.1 Annual Land-Cover Maps 19
3.2 Annual Cropland Change 23
3.3 Overlay with Conflict Data 26

4 Discussion **27**

5 Conclusions **32**

EPILOGUE **33**

REFERENCES **34**

Appendix **39**

1 Introduction

Mozambique is one of the world's "invisible emergencies" (UNHCR, 2022). Especially Mozambique's most northern province, Cabo Delgado, suffers from poverty and unemployment, and is often referred to as a "forgotten province" (Neethling, 2021). This has fuelled the emergence of an Islamic insurgency that has swept across the region since October 2017, resulting in the displacement of hundreds of thousands of people (UNHCR, 2022). The conflict has its roots in the socio-economic marginalisation of northern Mozambique. The inequalities worsened by the discovery of minerals and natural gas deposits and facilitated the armed group's recruitment in the region (ACAPS, 2023). The government of Mozambique responded by deploying state forces and collaborating with regional and international allies including the Southern African Development Community's Mission in Mozambique (ACAPS, 2023). The conflict has been intensifying over the years and is still ongoing, leading to insecurity, food shortages, and displacement.

Furthermore, Mozambique's north is affected by the devastating impacts of climate change. Only within the first few months of 2022, three major cyclones hit the provinces, affecting around one million people (ACAPS, 2022).

As a consequence of the ongoing armed conflict and the impacts of climate change, around one million people have been displaced within the country, according to the UNHCR (2022) and IOM (2022). This trend appears to be weakening in 2023 with an increasing number of returnees: about 541,000 were counted in the 19th round of Mobility Tracking Assessments (IOM, 2023). However, IOM (2023) still counted a total of 627,846 IDPs in Cabo Delgado (see Figure 1). Moreover, due to the remoteness of some locations and the heavily politicized environment, with limited press freedom, there is only limited access to information about the conflict's impact on the country's population (ACAPS, 2023). It is estimated that, from November 2022 to March 2023, 690,400 people in Cabo Delgado experienced 'Crisis' (IPC Phase 3) or worse food insecurity, mainly resulting from the conflict and natural disasters (such as cyclones). Due to a lack of data, these numbers do not include eight of the 17 districts in Cabo Delgado which are most conflict-affected and arguably among the most food insecure (IPC, 2023).

In a context like Mozambique's with conflict zones that are considered a "no-access" or "hard-to-reach" site, the analysis of remotely sensed data can provide a comprehensive overview of the situation on-site. It can provide critical and timely information about agricultural performance and possible food insecurity (Kerner et al., 2020). A reduction of active cropland might indicate displacement of people. Early recognized, it can help monitor the conflict and organize humanitarian aid where needed.

However, the timely and accurate creation of high-resolution cropland maps and cropland abandonment maps is challenging, especially in regions that are dominated by smallholder farming, like Mozambique. The availability of accurate and readily accessible ground truth data that is necessary for training and validating predictive models is not given in many of these regions. Especially, if a rapid response is needed within a crisis (Kerner et al., 2020). Cropland mapping in Mozambique is further challenged by a high prevalence of cloud cover in the crop growing seasons which calls for a high temporal resolution

of satellite imagery to provide a profound data availability (Rufin et al., 2022).

This study aims to assess the impacts of the ongoing conflict in Cabo Delgado on cropland abandonment as an indicator of population displacement and food insecurity. In the first step, some techniques of automatic cropland detection are tested, and cropland abandonment maps are produced. Next, these maps are compared to existing datasets like ESA Worldcover (Zanaga et al., 2021, 2022) and ESRI Land-Cover (Karra et al., 2021). Finally, the maps are overlayed with conflict data (e.g. ACLED, 2023) to connect the conflict with cropland change.

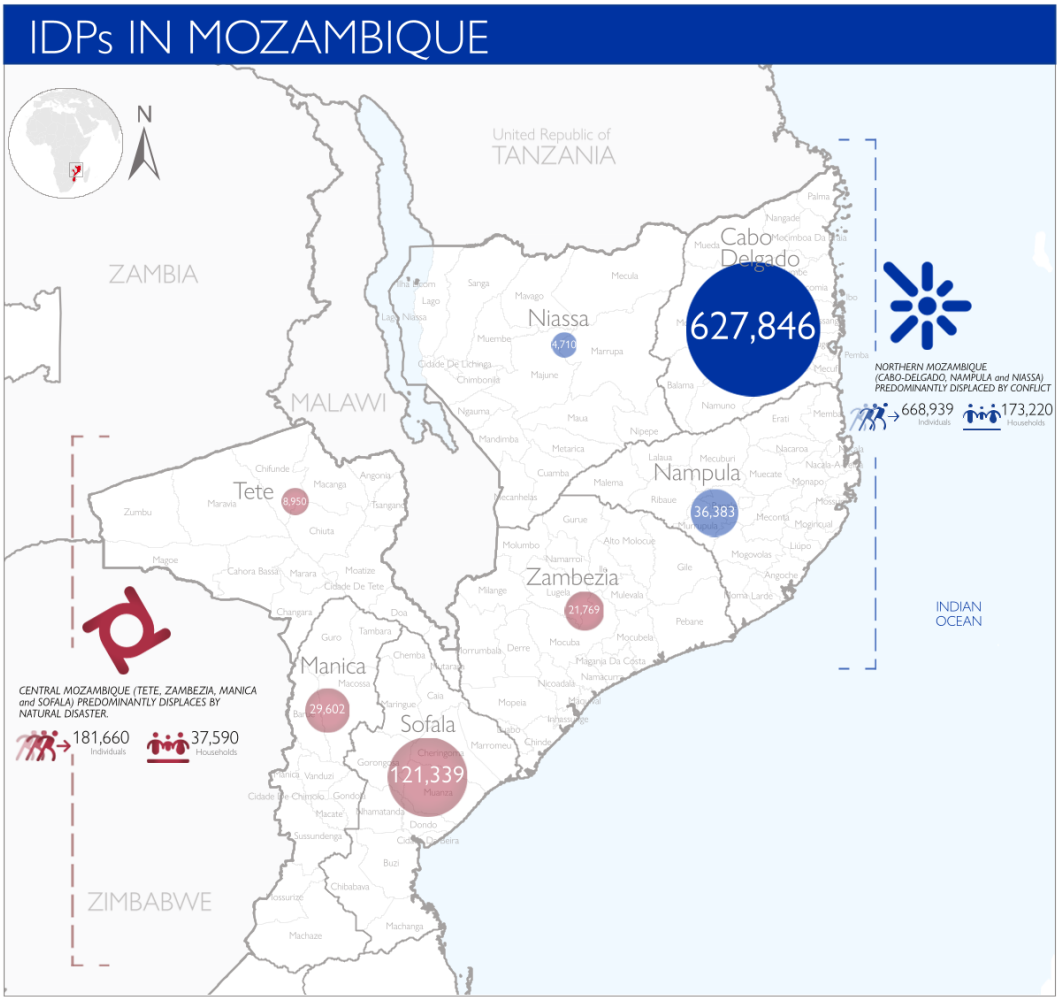

Figure 1: Northern and central Mozambique, IDPs per district (IOM, 2023)

In the following paragraphs, some studies are presented that followed different approaches to detect cropland abandonment. They will be described only in little detail to focus on the main methodological techniques that the present study has adopted.

In 2019, the World Food Programme (WFP) used Earth Observation data in hard-to-reach areas in Mali to assess the physical impacts of the conflict in the region of Mopti (WFP, 2020). The detection of cropland abandonment triangulated with insecurity data showed a clear correlation between agricultural decline and violent events. Methodologically, WFP (2020) used Sentinel-2 images with a spatial resolution

of 10 meters as well as a dataset of populated sites based on data from the Malian Institute of Statistics (INSTAT) and additional ancillary data. The study acquired Sentinel-2 images during the agricultural season (June 15th to October 15th) for 2016, 2017, 2018, and 2019 and produced NDVI composites for each year. The detection of cropland abandonment was finally done manually by visually comparing these composites from different years. As a result, the authors classified each populated site into one of five different cropland change categories (WFP, 2020).

Based on this methodology, CEMS (2020a) started a series of analyses for Nigeria with updates in CEMS (2020b), CEMS (2021), and CEMS (2022). The goal was to estimate the impact of the conflict and to estimate the population affected by cropland loss in an area that has not been accessed for several years. The first report (CEMS, 2020a) used the years 2010 and 2019 as reference years and five different AOIs. The subsequent reports (CEMS, 2020b, 2021, 2022) changed their temporal and/or spatial scope in different ways, the methodology, however, remained the same throughout all reports. The studies used Sentinel-2 satellite imagery. Limited data availability due to cloud cover was faced by adding Landsat-8 data, extending the time period, or computing median NDVI values. The imagery was acquired according to the Nigerian crop calendar with averages for three parts of the growing season per year that were combined as an NDVI RGB composite. "Due to the extremely heterogeneous data situation (different sensors, unsteady timeline of data, poor coverage)", analysis of crop change detection was done on a visual basis only (CEMS, 2022, p. 15).

Another study has been recently made by the Food and Agriculture Organization of the United Nations to assess changes in land-cover and identify priority areas that are most affected in the provinces of Nampula and Cabo Delgado of Mozambique (Jalal et al., 2022). The authors mapped seventeen land-cover classes based on the national land-cover map of 2016, provided by the Fundo Nacional de Desenvolvimento Sustentavel (FNDS) of Mozambique. Training data had been collected from this map (spectral outliers excluded) and used in an object-based image analysis approach (OBIA) to create image objects of Sentinel-2 imagery that have subsequently been classified using an RF classifier. Finally, Jalal et al. (2022) detected land-cover changes by the image differencing method which is an algebra-based change detection approach (Lu et al., 2004). One of the major shortcomings of this study was the lack of accurate ground data. To overcome this, the authors scaled the results at admin level 3 (Posto).

These studies provide useful insights into the detection of cropland abandonment and its connection to conflicts. However, to use cropland abandonment as an indicator of population displacement and food insecurity as a rapid response tool, the automation of active and abandoned cropland detection would be favourable. In regions where irrigated agriculture is predominant, this is much easier since the growing cycle of crops is undisturbed. However, rain-fed agriculture accounts for most of the farmed land in low-income countries like Mozambique. Climate change, and with it the increased weather variability, leads to a higher vulnerability of rain-fed agriculture and also a higher variability of the crop cycle. Rain-fed agriculture is therefore much more difficult to detect automatically on satellite imagery.

However, quite many studies exist that tried to automate the process of detecting cropland and its abandonment. They use a variety of different datasets including Landsat, Sentinel-2, Sentinel-1, and MODIS

NDVI. Machine learning techniques have been widely used to identify cropland in Earth Observation data. Very common are tree-based classifiers (primarily random forests or decision trees) and neural network/deep learning methods (primarily recurrent or convolutional neural networks) (Kerner et al., 2020).

Some local studies exist that aim to map cropland in Mozambique. In a recent study, Rufin et al. (2022) mapped active cropland and short-term fallows in the smallholder landscape of Mozambique, following a fully automated approach with Google Earth Engine. The authors used PlanetScope 4-band (Red, Green, Blue, NIR) surface reflectance mosaics (hereafter PlanetScope mosaics) with a spatial resolution of 4.77 m provided through Level 1 access of the NICFI data program (Planet Labs Inc., 2023), available monthly from September 2020 onwards, and applied an iterative active learning scheme for training data collection, model parametrization, and classification, reaching high overall accuracy levels of around 90% (Rufin et al., 2022).

In another study about cropland in Mozambique, Bey et al. (2020) compared the accuracies of different pixel-based composites of Landsat-8 imagery to classify and characterize land-use change in Gurué District. They focused on the distinction between small-scale and large-scale cropland, analysing the recent growth of foreign investments in agriculture in Mozambique. Ground-truth data has been collected through field campaigns; image classification (using RF) and change detection (post-classification) have been performed using Google Earth Engine. The Median composite performed best in terms of cloud-, shadow- and haze-removal and general visual consistency (Bey et al., 2020).

Yin et al. (2018) and Yin et al. (2020) developed new approaches to detect the extent and timing of cropland abandonment using Landsat time series. Yin et al. (2018) followed a combined spatial and temporal segmentation approach for one Landsat footprint in the Caucasus in which they first performed an object-based multi-resolution spatial segmentation to create spatially homogeneous objects. Secondly, they estimated agricultural land probability for each object by summarizing the per-pixel probability estimated from an RF model. Finally, they created temporal segments at the object level by applying a temporal segmentation algorithm on the agricultural land probability time series to identify change classes and detect where abandonment occurred. Yin et al. (2020), on the contrary, developed a per-pixel classification approach using the entire Landsat time series from 1987 to 2007 and tested this approach in 14 study regions across the globe. The authors produced annual land-cover classifications using training data derived from calibration samples that were stable in terms of their land-cover from 1986 to 2018. To detect cropland abandonment, they used a post-classification comparison and detected pixels with stable resp. changing land-cover. Abandoned cropland was defined as a pixel that was classified as non-cropland for at least five consecutive years. Cropland that was not actively managed consecutively for less than five years was mapped as fallow, following the definition of FAO (Yin et al., 2020).

One of the main challenges for crop mapping in a smallholder landscape like Mozambique's is the availability of ground truth data for training and validation of classification models. Kerner et al. (2020) present a method for rapid mapping of croplands in regions where little to no ground data is available (here Togo). The authors leveraged a combination of global and local datasets with crowd-sourced and

active labelling respectively. Together with their approach of using a multi-headed Long Short-Term Memory (LSTM) network to learn local and global features for identifying cropland based on multi-spectral time-series Sentinel-2 surface reflectance (Level 2A) observations, they reached high accuracies (83%).

Another approach has been followed by Bofana et al. (2020). The authors compared four different classifiers with Landsat-8 and Sentinel-2 data in a zone-specific classification for cropland mapping over four different agroecological zones (AEZ) in the Zambezi River basin (ZRB). Training data was derived from three existing land-cover datasets to minimize the cost of sample acquisition over the large area. The study reached high accuracies with the Random Forest classifier with an average overall accuracy of 87.4% across the four AEZs. The authors concluded that a sample extraction over full agreement areas among existing datasets provided reliable calibration sets that can replace costly in situ measurements (Bofana et al., 2020). Therefore, the present study follows a similar approach regarding the acquisition of training data.

Many studies use tree-based classifiers, like e.g. Samasse et al. (2020). The authors used existing land-cover training data for 2013 with cloud-free Landsat-8 images (for 2013-2015) to train locally optimized Random Forest models predicting the presence or absence of cropland across the non-dessert land area of the West African Sahel zone. The training data was taken from the West Africa Land-Use Land-Cover Time Series for 2013 using the Rapid Land-Cover Mapper (RLCM), a project led by the US Geological Survey (Tappan et al., 2016). Further, Samasse et al. (2020) calculated four vegetation indices (NDVI, EVI, SAVI, MSAVI) as predictor variables for the Random Forest classification, in which they used Out-of-bag (OOB) error estimation during the training process to fine-tune RF model parameters and provide internal cross-validation before independent accuracy assessment (Samasse et al., 2020, p. 5). The authors generated a 100x100 km grid over the study area and classified each grid cell independently. The study reached accuracies of around 80% with the lowest values in Mauritania which is probably due to particularly small-sized farms and low intensity of agriculture. The classified cropland class included short-term fallow fields but excluded long-term fallow (or abandoned) areas (Samasse et al., 2020).

Tong et al. (2020) used Google Earth Engine and a Random Forest classifier to process Sentinel-2 imagery to detect fallow fields across the Sahel within cropland mapped by Copernicus Dynamic Land-Cover map at 100 m resolution from 2015. The authors used a two-step automated approach to generate a reference dataset needed for training and validation. With the help of seasonal metrics from MODIS NDVI for 2017, the authors defined the period representing the maximum spectral difference between cropped and fallow fields which is around the dry-down period of the growing season. This period was then used to define the start and end of the relevant Sentinel-2 imagery acquisition period. Tong et al. (2020) differentiate between cropped and fallow fields, and while not precisely defining fallow fields, they regard only one full year and use the spectral differences between cropped and fallow fields. In this case, fallow means not cropped within one year.

This leads to an important question regarding the definition of abandoned areas. Since crop-fallow rotation practices are integral parts of land management strategies, especially in regions where other

options to restore soil fertility such as chemical fertilizers or livestock manure are limited (Tong et al., 2020), it is essential to precisely define the characteristics that distinguish short-term fallow fields that are part of crop-fallow rotations and long-term fallow fields that can be assumed to have been abandoned. According to the FAO, agricultural land abandonment is defined as agricultural land that has not been used for a minimum of two to five years. However, in multi-year crop rotation systems, the fallow periods might be prolonged (Yin et al., 2018). Likewise, in a conflict situation, the abandonment of cropland might only last for a short time, depending on the perceived danger from the conflict. Hence, in the present study, abandoned fields are defined as fields that have not been cropped within one agricultural year. The class cropland includes only actively cropped fields with the assumption that all areas that change from cropland to another class from year to year are abandoned fields. In a quickly changing conflict situation, like the one in focus, this is a reasonable assumption even if it might include some fields that lie fallow within the regular crop rotation system.

Cropland abandonment can either be detected by classifying abandoned fields directly (Estel et al., 2015; Löw et al., 2018; Rufin et al., 2022; Tong et al., 2020) or by performing a change detection approach that identifies differences in the state of an object or phenomenon by observing it at different times (Basnet & Vodacek, 2015; Eklund et al., 2017; El-Hattab, 2016; Olsen et al., 2021; Yin et al., 2020). There are several change detection techniques in remote sensing. Lu et al. (2004) provide a comprehensive overview. Many studies use the post-classification comparison approach which compares separately classified multi-temporal images.

Olsen et al. (2021) conducted a study about the impact of conflict-driven land abandonment on food insecurity in South Sudan. Their approach to detecting abandoned cropland used data-fusion of Sentinel-2, Landsat-8, and MODIS imagery besides a Copernicus land-cover product of 2016 as a proxy for broad land-cover and climatic patterns. The authors also included Sentinel-1 VV and VH time series. They produced land-cover classifications for 2016, 2017, and 2018, and detected cropland dynamics subsequently through post-classification change detection. In a study from 2015, Basnet & Vodacek (2015) developed a process to monitor the spatial and temporal land use/land cover changes in the Lake Kivu region in Central Africa. After performing a supervised classification on Landsat imagery supplemented with ancillary data, a pixel-based post-classification change detection approach has been performed. The authors used the ENVI 4.7 software for change detection. El-Hattab (2016) used the cross-tabulation technique which is a method within the post-classification approach to determine land-cover changes in Egypt. Eklund et al. (2017) investigated the effects of a conflict on agricultural land use using the example of the Islamic state in Syria. They classified annual land use maps for the years 2000-2015 and tracked the dynamics of cropland by comparing a long-term reference period (most common class from 2000 to 2013) as well as a short-term period (class in 2013) with the class in 2015.

The present study follows the post-classification comparison approach to detect changes in croplands. The abandonment of cropland is determined from year to year, taking into account fields that lie fallow in the crop rotation cycle. Even if this might not be the common definition of cropland abandonment, it considers the suspected quick changes that can happen in the light of the present conflict.

To better understand the correlation between conflicts and cropland abandonment, the present study compares the produced change maps with conflict data provided by ACLED (2023). Similarly, Yin et al. (2019) investigated how the distance to conflicts and the intensity of the conflict, measured as the number of conflicts and the number of casualties, affected agricultural land abandonment and subsequent re-cultivation, by combining social, environmental, and economic variables with remotely sensed maps of agricultural change. The authors used logistic, fixed-effects, and random-effects regression models to explain agricultural land abandonment between 1989 and 1998 in the northern Caucasus. Olsen et al. (2021) used propensity score matching to show the statistical relationship between cropland abandonment and armed conflict in South Sudan.

In summary, the present study uses a combination of approaches (training samples from existing datasets, RF classification in Google Earth Engine, post-classification change detection, and correlation with conflict data) to identify cropland abandonment in the light of the ongoing conflict in the region of Cabo Delgado in Mozambique. The materials and methods that have been used are described in detail in section 2.

2 Materials and Methods

The complete workflow of this analysis is shown in Figure 2. The analysis included data acquisition (Section 2.2), pre-processing (Section 2.3), generation of training and validation data (Section 2.4), image classification (Section 2.5), accuracy analysis (Section 2.6), change detection steps (Section 2.7), and overlay with conflict data (Section 2.8). Each step is described in detail in the following sections. Section 2.1 provides an overview of the study area, the northernmost province of Mozambique, Cabo Delgado.

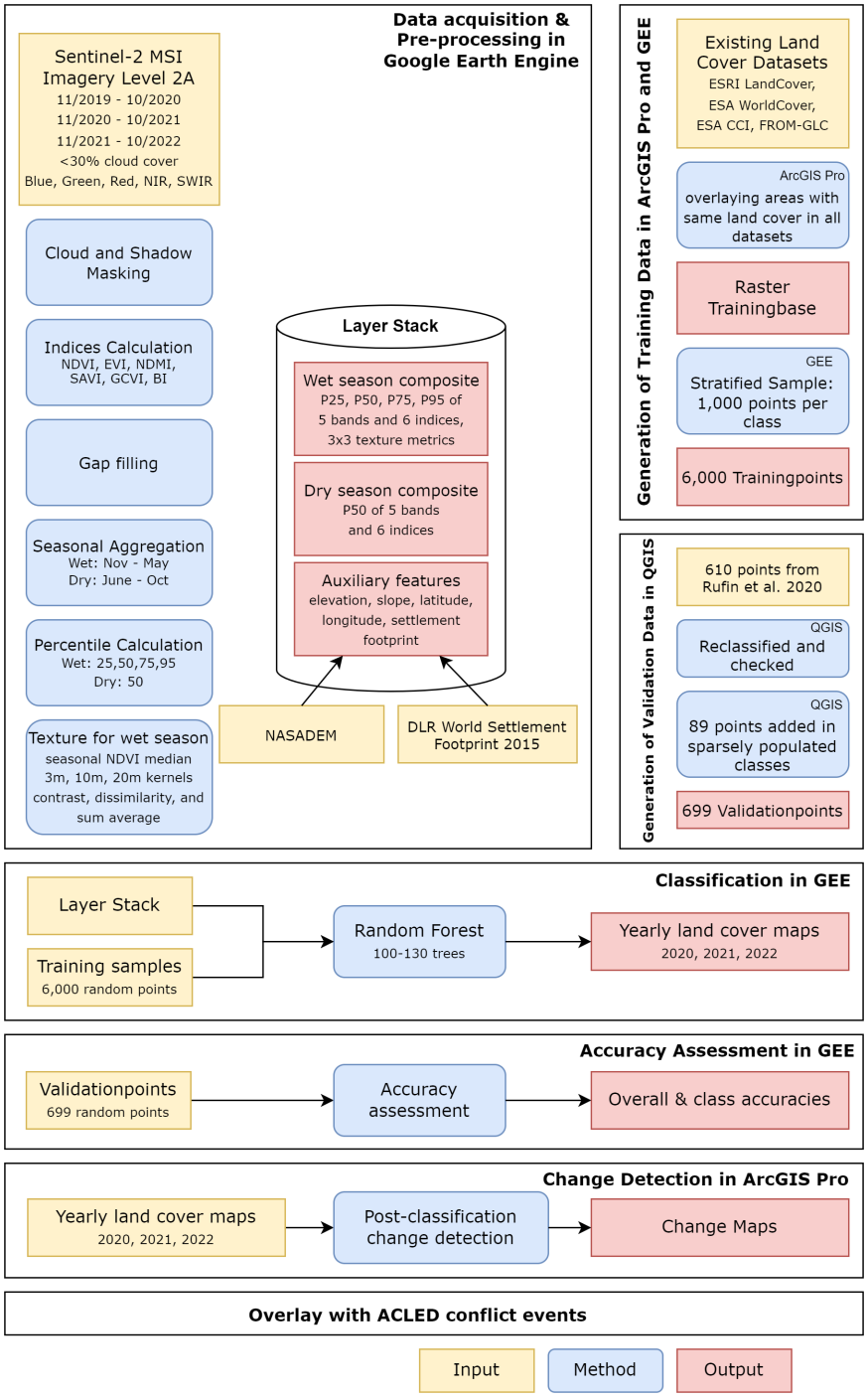

Figure 2: Workflow

2.1 Study Area

The province of Cabo Delgado (10.49-14.02°S, 37.97-40.60°E) is located in the northernmost part of Mozambique, bordering the United Republic of Tanzania. It has an area of 82,625 km² and a population of 2,333,278 in 2017 with the majority of the population living in rural areas (Government of Cabo Delgado Province, 2017; National Institute of Statistics, 2023). The province is only sparsely populated with an average population density of 28.2 persons per km². However, most of the population is concentrated in the south of the province with the highest population density of around 2,000 people per km² in the province capital Pemba Cidade (see Figure A1).

The region is dominated by the Eastern Miombo Woodlands which is an ecoregion of grass- and woodlands in northern Mozambique, southern Tanzania, and south-eastern Malawi. Hence, the province's land-cover is dominated by rangeland and dispersed forests. Cabo Delgado's east borders the Mozambique Channel of the Indian Ocean. In the north, the Rovuma River forms the border with the United Republic of Tanzania. The south border to its neighbouring province Nampula is marked by the Lurio River. Another major river running through Cabo Delgado is the Messalo River. Cabo Delgado's rivers are characterized by seasonal flows and lined by swamps and subsistence agriculture. The terrain is mostly of low elevation and rises gently from east to west, from the eastern coast to the high plains, with some local topographical features (see Figure A1).

Cabo Delgado has a tropical climate that follows the seasonal migration of the inter-tropical convergence zone, hence resulting in distinct hot wet (November to April) and cool dry (May to October) seasons. The temperatures have an average annual of 25°C with an average low of 21°C and an average high of 27°C (Government of Cabo Delgado Province, 2017). Precipitation varies between 700 and 1500 mm per year and is highest in the northern coastal region while the south around the city of Pemba is the driest. Cabo Delgado is located in the tropic warm/sub-humid Agro-Ecological Zone (AEZ) for Africa south of the Sahara (HarvestChoice & Institute (IFPRI), 2016) (see Figure A1).

According to the seasonal calendar of Mozambique (Famine Early Warning Systems Network, 2013), northern Mozambique has three main agricultural seasons: land preparation in September to November, planting and lean season during the rainy season from November to March, and harvest season from April to July (see Figure 3).

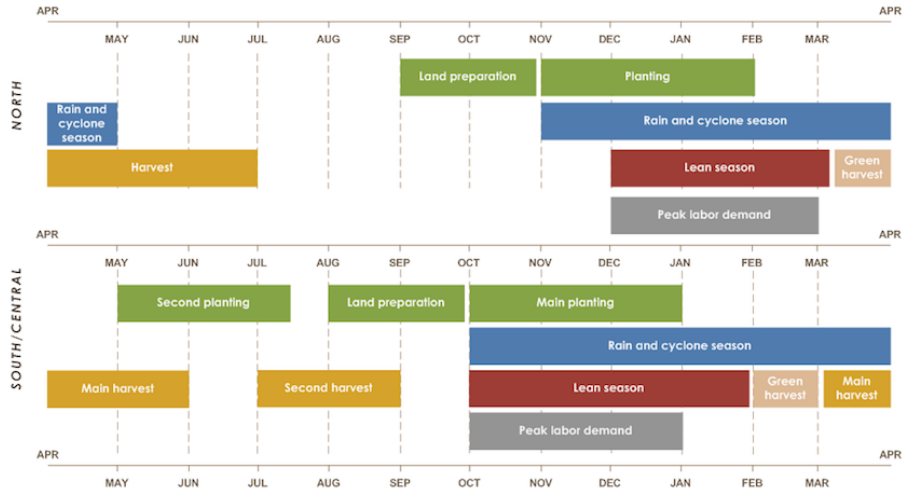

Figure 3: Seasonal calendar, typical year in Mozambique (Famine Early Warning Systems Network, 2013)

Agriculture is an important source of income, dominated by low-intensity smallholder agriculture with high labour demands, little to no access to fertilizers, and frequent fallow rotations. Hence, the productivity is low due to a lack of appropriate technologies and a general inaccessibility of markets for smallholder farmers (IFAD, 2023; Rufin et al., 2022). According to Lesiv et al. (2019), most fields in Cabo Delgado are very small fields with an area less than 0.64 ha which results in field side lengths of between 50 and 100m.

2.2 Data

This work used Sentinel-2 imagery on processing level 2A that has been accessed within Google Earth Engine (GEE). "The Level-2A processing includes a Scene Classification and an Atmospheric Correction applied to Top-Of-Atmosphere (TOA) Level-1C orthoimage products. Level-2A main output is an orthoimage atmospherically corrected, Surface Reflectance product." (ESA (n.d.-b)) On processing level 2A, S2 imagery is available from January 2019 onwards. To have a consistent and comparable data basis for the analysis, Sentinel-2 imagery has been used to evaluate three consecutive years:

- 2020: November 1st, 2019 to October 31st, 2020
- 2021: November 1st, 2020 to October 31st, 2021
- 2022: November 1st, 2021 to October 31st, 2022

This cycle has been chosen in accordance with the crop calendar in northern Mozambique (see Figure 3) with the assumption that the wet season is from November to May and the dry season from June to October.

2.3 Pre-Processing

All pre-processing was done in Google Earth Engine. The acquired Sentinel-2 images were filtered by Region of Interest (ROI), date according to the outlined yearly cycles and cloudy pixel percentage lower 30%, and stacked into image collections per year. For the analysis, only the Blue, Green, Red, NIR and

SWIR bands (see Figure 4 for information on Sentinel-2 bands) were selected. Further, the images were cloud-masked using the Sentinel-2 quality band at 60m resolution (Q60) and the Sentinel-2 SCL band for Scene Classification at 20m resolution.

Bandnumber	Name	Central wavelength (nm)	Bandwidth (nm)	Spatial resolution in m
2	Blue	492.7	65	10
3	Green	559.8	35	10
4	Red	664.6	30	10
8	NIR	832.8	105	10
11	SWIR	1613.7	90	20

Figure 4: Sentinel-2 MSI used bands and their spectral resolutions (ESA, n.d.-a)

The study area is covered by 17 S2 UTM tiles, each with a surface of 110 x 110 km² (see Figure 5). Figure 6 shows the number of images that are available for the respective season and year after filtering.

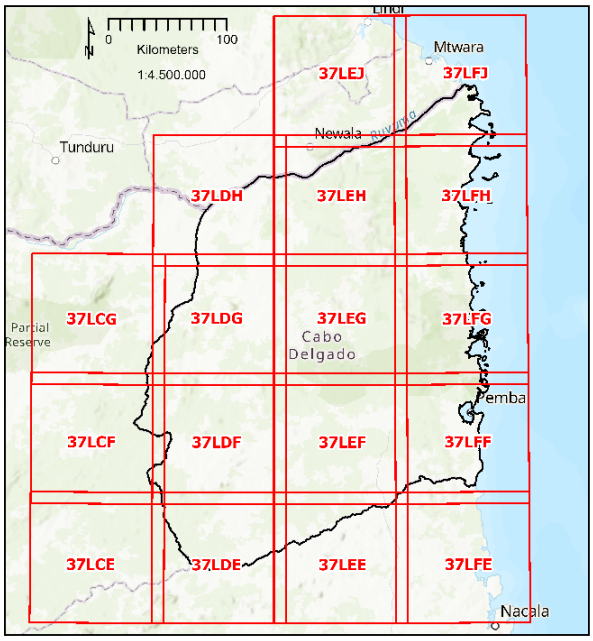

Figure 5: Sentinel-2 UTM tiles over Cabo Delgado (ESA, n.d.-a)

Year	Season	Months	Number of images with cloud cover < 30%	% of images used	Number of images total
2019/2020	Wet	November - May	344	36.91	932
	Dry	June - October	501	71.88	697
2020/2021	Wet	November - May	362	39.43	918
	Dry	June - October	480	67.32	713
2021/2022	Wet	November - May	349	37.13	940
	Dry	June - October	442	66.67	663

Figure 6: Number of Sentinel-2 observations per year and season

Remote sensing derived vegetation indices are widely used in addition to individual band reflectances to detect vegetation and its condition. This is mostly based on the strong capability of vegetation to reflect the NIR band (Samasse et al., 2020). In this analysis, the following six indices were derived to add information to the remote sensing data: NDVI (Normalized Difference Vegetation Index), EVI

(Enhanced Vegetation Index), NDMI (Normalized Difference Moisture Index), SAVI (Soil Adjusted Vegetation Index), GCVI (Green Chlorophyll Vegetation Index), and BI (Bare Soil Index). Figure 8 shows the equations used for calculation.

While the NDVI is extensively used in satellite remote sensing based vegetation analysis, it gets quickly saturated in high biomass surfaces. The EVI allows the correction of this saturation effect. It also corrects atmospheric effects of aerosol by including the blue band in the calculation. The formula includes a gain factor (here 2.5), two coefficients of the aerosol resistance term (here 6 and 7.5), and a soil-adjustment factor (here 1). This study used the coefficients adopted in the MODIS EVI algorithm like other studies before (Jalal et al., 2022; Morell-Monzó et al., 2020; Samasse et al., 2020). The NDMI is sensitive to soil and vegetation moisture, it is calculated by using the SWIR band instead of the NIR Band (Morell-Monzó et al., 2020). The SAVI compensates for the effects of soil background in sparsely vegetated areas by including a soil adjustment factor. The value 0.5, that was chosen in this work, has been found to reduce soil noise for a wide range of vegetation classes (Huete, 1988). The GCVI is known to capture greater areas of vegetation and has been successfully used in the estimation of leaf area index and green leaf biomass (Bey et al., 2020; Bofana et al., 2020; S. Xiong et al., 2022). Finally, the BI captures the soil signal when croplands are tilled or harvested. Higher values indicate higher soil bareness (Bofana et al., 2020; Yin et al., 2020).

After calculation of indices, a 12-day moving window was used to fill gaps and to smooth the time-series for each year.

Subsequently, the images were filtered and aggregated by season with the assumption that the wet season is from November to May and the dry season from June to October (see section 2.1).

Based on the literature review, to avoid cloud contamination problems, the 25%, 50%, 75%, and 95% percentiles were calculated to compose seasonal composites (Bofana et al., 2020). Besides correcting for cloud contamination, the calculation of four percentiles offers the advantage of fully capturing phenological vegetational information.

In recent studies, textural features have been shown to add value to the classification process since abandoned agricultural land is rather uneven and has a rough texture compared to the uniformity and smooth texture of active agricultural land (Bey et al., 2020; Olsen et al., 2021; Rufin et al., 2022). Therefore, the 'grey-level co-occurrence matrix' textural features 'contrast', 'sum average' and 'dissimilarity' were calculated for the wet season (November - May) with three different kernels of 3, 10 and 20 pixels. These features have been proposed by Haralick et al. (1973) and Conners et al. (1984) and have shown the highest importance values for the following RF classification.

The yearly stack image that was used for the classification was obtained by stacking the wet and dry seasons composites and adding the auxiliary features elevation and slope (both obtained from the NASADEM (NASA JPL, 2020) in GEE), latitude and longitude as well as World Settlement Footprint 2015 (Marconcini et al., 2020). In total, 102 features were included in the image stack for further classification (see Figure 8).

2.4 Training Data Generation

Since the ROI is located in a conflict zone which is considered a "no access/hard to reach area", the acquisition of ground truth reference data, which is needed for a supervised classification such as the one pursued here, is particularly challenging. One goal of this thesis is to find a reliable method to automatically detect the shift of croplands as an indicator of displacement and food insecurity. Therefore, also the acquisition of reference data should be automated.

One option, that is tested here, is to obtain training and validation data from existent land-cover datasets. This approach has been followed by Bofana et al. (2020) who found that uncertainty was reduced, and reliable calibration sets were created by extracting samples over "full agreement areas among existing datasets" (Bofana et al., 2020, p. 1f.).

A stack of nine publicly available land-cover datasets were used to collect reference samples:

1. ESA Worldcover, 10m resolution, available for 2020 and 2021 (Zanaga et al., 2021, 2022)
2. ESRI Land-Cover, 10m resolution, available for 2017, 2018, 2019, 2020 and 2021 (Karra et al., 2021)
3. FROM-GLC: Finer Resolution and Observation and Monitoring of Global Land-Cover, 10m resolution for 2017 (Gong et al., 2019)
4. ESA Climate Change Initiative (CCI): S2 prototype LC map at 20m resolution of Africa 2016 (ESA, 2017)

ESA Worldcover maps have global coverage and reach an overall accuracy of 74.4% for v100 (2020) and 76.7% for v200 (2021) (Tsendbazar et al., 2021). Their creation built further on ESA's experiences with GlobCover and CCI Land-Cover. The algorithm used to generate the maps is based on the algorithm to produce the dynamic yearly Copernicus Global Land Service Land-Cover (CGLS-LC) map with 100m resolution. The maps represent the land-cover for 2020 and 2021 respectively, from January 1st to December 31st. Sentinel-1 and Sentinel-2 data covering the reference year were used for the creation. Crops are defined as "Land covered with annual cropland that is sowed/planted and harvestable at least once within the 12 months after the sowing/planting date. The annual cropland produces an herbaceous cover and is sometimes combined with some tree or woody vegetation. Note that perennial woody crops will be classified as the appropriate tree cover or shrub land-cover type. Greenhouses are considered as built-up." (Zanaga et al., 2021, 2022) The changes between v100 and v200 are both due to the improvements made in the classification algorithm and the dynamics between the two years.

ESRI Land-Cover maps also have a global coverage and reach an overall accuracy of 85% (ESRI, 2021), generally similar for each year from 2017-2021. Each annual map is produced by using a whole year's Sentinel-2 observations. The maps are available from ESRI's "ArcGIS Living Atlas of the World". Crops are defined as "Human planted/plotted cereals, grasses, and crops not at tree height; examples: corn, wheat, soy, fallow plots of structured land." (ESRI ArcGIS Living Atlas of the World, 2022)

The Finer Resolution Observation and Monitoring of Global Land-Cover (FROM-GLC) is the first 10m resolution global land-cover map produced using Landsat Thematic Mapper (TM) and Enhanced

Thematic Mapper Plus (ETM+) data (Gong et al., 2019). Croplands are not further defined. The dataset reaches an overall accuracy of 72.76% (Gong et al., 2019).

Finally, the ESA CCI Land-Cover map has a regional coverage, mapping land-cover in Africa. The validation of the map has been performed by the International Institute for Applied Systems Analysis (IIASA) in the frame of CrowdVal project, using crowd-sourcing and innovative approaches (IIASA, 2019). While a previous validation showed an overall accuracy of 64% (Lesiv et al., 2017), IIASA (2019) validated four countries separately (Kenya, Gabon, Ivory Coast and South Africa) with varying results from 44% for South Africa, 47% for Ivory Coast, 56% for Kenya to 91% for Gabon. These results show the highly fragmented land-cover situations within those countries, with Gabon having a high amount of tree cover. According to a map presented by Lesiv et al. (2017) (p.14), the spatial accuracies in Cabo Delgado are between 46 and 65%.

It was anticipated to use further land-cover maps, for example the GFSAD30 product which is the result of the Global Food Security-Support Analysis Data Project at 30 m resolution funded by NASA (J. Xiong et al., 2017). Although the map resulted in very high accuracies, it could not be used in this analysis due to its limitation to only three classes (water, non-cropland, cropland). Similar reasons led to the disregard of other interesting land-cover datasets (e.g. Dynamic World: based on single images, accuracies for croplands low (Brown et al., 2022)).

In order to be able to generate consistent reference samples, the chosen datasets needed to be harmonized into the desired land-cover classes. Figure 7 shows the lookup table between the original and final land-cover classes for each dataset.

Final Classes	**Original Classes**			
	FROM-GLC Finer Resolution Observation and Monitoring of Global Land Cover 2017 10m	*ESA CCI Land Cover Africa 2016 20m*	*ESA WorldCover 2020, 2021 10m*	*ESRI LandCover 2017, 2018, 2019, 2020, 2021, 2022, 2023 10m*
Cropland (1)	Cropland (10)	Cropland (4)	Cropland (40)	Crops (5)
Forest (2)	Forest (20), Shrub (40)	Trees (1), Shrubs (2), Vegetation aquatic or regularly flooded (5)	Tree Cover (10), Shrubland (20), Mangroves (95)	Trees (2), Flooded vegetation (4)
Grassland (3)	Grass (30)	Grassland (3), Lichen Mosses / Sparse vegetation (6)	Grassland (30), Herbaceous wetland (90), Moss and lichen (100)	Rangeland (11)
Built-up (4)	Impervious (80)	Built up Areas (8)	Built-up (50)	Built area (7)
Water bodies (5)	Water (60), Snow/Ice (100), Cloud (120)	Open water (10), Permanent snow and/or ice (9)	Snow and Ice (7), Permanent water bodies (80)	Water (1), Snow/Ice (9), Clouds (10)
Bareland (6)	Bareland (90)	Bare areas (7)	Bare/sparse vegetation (60)	Bare ground (8)

Figure 7: Land-cover classes conversion lookup table

To obtain training points, the chosen land-cover maps were overlayed, using ArcGIS Pro, and only those pixels that were classified with the same land-cover class in all layers, were kept to produce a raster that was subsequently used to obtain stratified sampled training points (1,000 per class) in GEE.

2.5 Classification

The Random Forest (RF) algorithm was used in this work to classify the Sentinel-2 data for the years 2020, 2021, and 2022. The RF model, first developed by Breiman (2001), is an ensemble learning algorithm that can be used to predict both continuous (regression) and categorical (classification) responses. It is based on classification and regression trees (CART). The model consists of an ensemble of decision trees where each tree works as a separate classifier which predicts the class by using a random sub-sample of the training values. The final class prediction is chosen by a maximum vote. With this procedure, RF does not over-fit and is more robust against outliers in the training data. Additionally, RF can measure the importance of each input variable, which indicates the contribution to classification accuracy.

Figure 8 summarizes the features induced in the RF models. In total, the classifier was fed with 102 features including four percentiles for wet and dry season for five original bands and six derived RS indices, three texture indices for three different kernel sizes for median NDVI value of the wet season, as well as auxiliary data like elevation, slope, latitude & longitude, and settlement footprint.

Feature Name	Metrics per object	Index formula / Data source
Original bands		
B2, B3, B4, B8, B11	Dry Season: P25, P50, P75, P95 Wet Season: P25, P50, P75, P95	Sentinel-2 MSI Level 2A
Spectral indices		
NDVI	Dry Season: P25, P50, P75, P95 Wet Season: P25, P50, P75, P95	$NDVI = \frac{NIR - RED}{NIR + RED}$
EVI		$EVI = 2.5 * \frac{(NIR - RED)}{(NIR + 6 * RED - 7.5 * BLUE + 1)}$
NDMI		$NDMI = \frac{NIR - SWIR}{NIR + SWIR}$
SAVI		$SAVI = \left(\frac{NIR - RED}{NIR + RED + L}\right) * (1 + L)$
GCVI		$GCVI = \left(\frac{NIR}{GREEN}\right) - 1$
BI		$BI = \left(\frac{(RED + SWIR) - (NIR + BLUE)}{(RED + SWIR) + (NIR + BLUE)}\right)$
Texture		
Contrast	Only for wet season: seasonal NDVI median, 3-, 10- and 20-pixels kernels	Grey-Level Co-Occurrence Matrix (GLCM)
Sum Average		
Dissimilarity		
Auxiliary features		
Elevation	Meters	NASADEM
Slope	Degrees	
Latitude & Longitude	Degrees	Google Earth Engine
Settlement Footprint	Binary raster: no settlement (0), settlement (255)	DLR World Settlement Footprint 2015

Figure 8: Input features for RF classifier

In first trials of classifying, bareland at the edges of rivers was often misclassified as built-up areas, which led to the inclusion of the settlement footprint.

These features were finally used in the training dataset to train a Random Forest model. Testing revealed that the ideal number of trees differs from year to year. Therefore, the classification of 2021 was done using 100 trees, and for 2020 and 2022 with 130 trees.

2.6 Accuracy Analysis and Validation

To validate the classifications, a sample of 699 random points were used. The majority of these points were taken from the training dataset of Rufin et al. (2022) that is openly available and of very high consistency and quality. The reference dataset used by Rufin et al. (2022) was filtered by ROI, since only samples in Cabo Delgado were of interest for this study (610 points). Since Rufin et al. (2022) assigned different classes, some of the points had to be reclassified and checked for their correct label. The general conversion table can be viewed in Figure 9. 89 validation points were then added to the sample to fill up the relatively sparsely populated classes 'built-up' (44), 'water' (31), and 'bareland' (14). The additional points were labelled with the help of Google Earth VHR images obtained in QGIS as well as S2 NDVI time series profiles obtained using the Google Earth Engine TimeSeries Explorer plugin for QGIS (Rufin et al., 2021). The final validation sample had 142 cropland points, 318 forest points, 93 grassland points, 50 built-up points, 50 water points, and 46 bareland points.

Class Rufin et al 2022	Validation Class
1: Active cropland	1: Cropland
2: Short-term fallow cropland	either 1: Cropland or 3: Grassland (decision made upon visual evaluation)
3: Herbaceous vegetation	3: Grassland
4: Open woodland	2: Forest
5: Closed woodland	2: Forest
7: Unvegetated	either 4: Built-Up or 6: Bareland (decision made upon visual evaluation)
8: Water	5: Water bodies

Figure 9: Conversion table for validation points

This validation sample was used to assess the accuracy of the produced land-cover maps for 2020, 2021, and 2022. For this, confusion matrices as well as common accuracy parameters like overall accuracy, user's accuracy, and producer's accuracy were calculated. Additionally, the F1-score was calculated (F1 = 2 x UA x PA/(UA+PA)) for each class. This score is a harmonic mean of user's and producer's accuracy that is more sensitive to imbalanced datasets (Kerner et al., 2020; Yin et al., 2020). The highest possible value of F1 is 1.0 which indicates perfect user's and producer's accuracies, and the lowest possible value is 0, if either the user's or producer's accuracy is zero.

2.7 Change Detection

Basnet & Vodacek (2015) detected land-cover changes using a pixel-based post-classification change detection algorithm. One advantage of a post-classification change detection method is its generation of not only change maps but also the identification of the nature (from-to) of land-cover change. One of the most popular approaches of post-classification change detection is bi-temporal change analysis of classified maps, which is the technique Basnet & Vodacek (2015) used. It is also leveraged in this master thesis.

To simplify the process and to provide a quick and easy evaluation of change, a hexagon raster was produced using ArcGIS Pro with a size of 5 km² per hexagon cell. For each hexagon, the share of cropland was calculated. Change in cropland was determined by calculating the change in cropland share between each year. This was done for the three own classifications made (2020, 2021, 2022) as well as for the ESA Worldcover datasets for 2020 and 2021 and the ESRI Land-Cover datasets for 2020, 2021 and 2022. As a result, five change rasters were produced:

- Own classification:
  - Change from 2020 to 2021
  - Change from 2021 to 2022
- ESA WorldCover:
  - Change from 2020 to 2021
- ESRI Land-Cover:
  - Change from 2020 to 2021
  - Change from 2021 to 2022

2.8 Overlay with Conflict Data

One purpose of this study was to analyse if the abandonment of cropland can be an indicator of population movements due to conflicts. This was done by obtaining georeferenced conflict data from the Armed Conflict Location and Event Data Project (ACLED) on political violence around the globe (Raleigh et al., 2023). The ACLED dataset contains disaggregated incident information on type, agents, location, date, and other characteristics of political violence, demonstrations, and select non-violent, politically-relevant developments in every country and territory in the world.

For this study, conflicts within Cabo Delgado and for the time of the current conflict starting in 2017 until today have been exported from the ACLED website (acleddata.com, 10.01.2024). Kept were only 'battles', 'violence against civilians', and 'explosions/remote violence', since those are presumably with the greatest impact on local population. 'Protests', 'riots', and 'strategic development' were excluded from the analysis. In total, 1,699 events were included, with the year 2020 being the most severe with 475 events. Figure 10 shows the total number of events per month over seven years (2017-2023). The majority of events were recorded for the years 2020 (475), 2021 (345), and 2022 (449), which represent the time-frame of this study. To be able to estimate a possible effect of these violent incidents on farming, the agriculturally relevant months are highlighted in orange in Figure 10. However, the decision of giving up fields to save your life might not be related to the stage of cultivation.

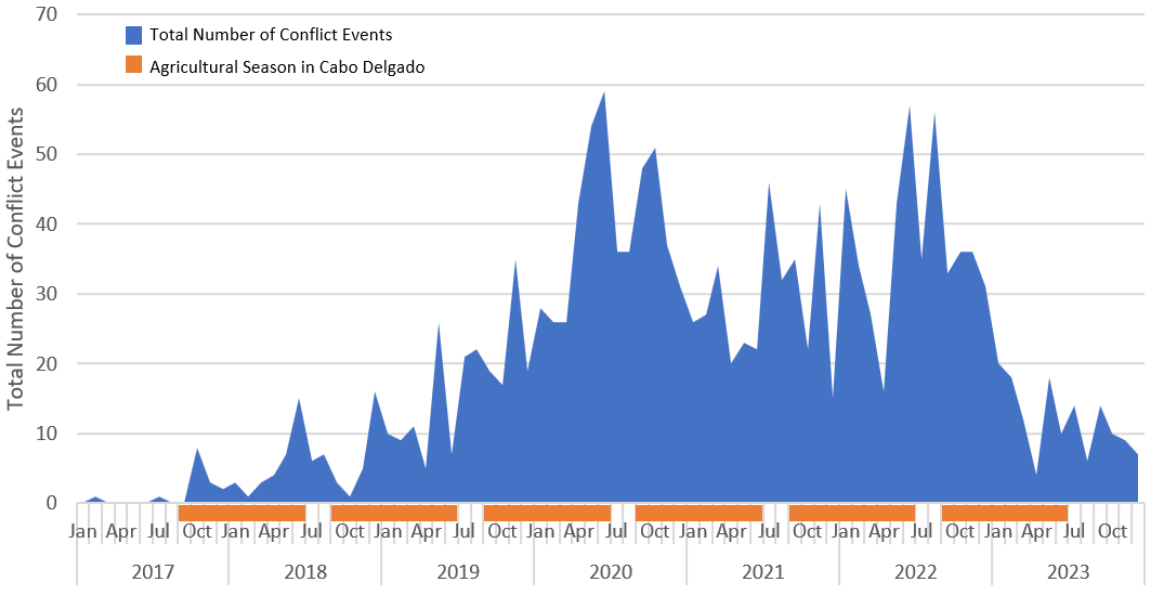

Figure 10: Number of conflicts in Cabo Delgado per month

3 Results

3.1 Annual Land-Cover Maps

The annual land-cover maps with a resolution of 10m per pixel look similar each year with only minor obvious changes. Agriculture was detected mostly in the south-western part of Cabo Delgado while the rest of the province seems to be mainly covered with forest and grassland (see Figure 11). Noticeable is an increase of forest in the centre of the province between 2020 and 2021, being reduced again from 2021 to 2022. Water and built-up areas seem to be in line with other land-cover products (e.g. land-cover and settlements in Figure A1). Bareland is the smallest class with only 0.23% of the pixels classified as bareland. It is mainly located along rivers and the shore and barely noticeable on the maps.

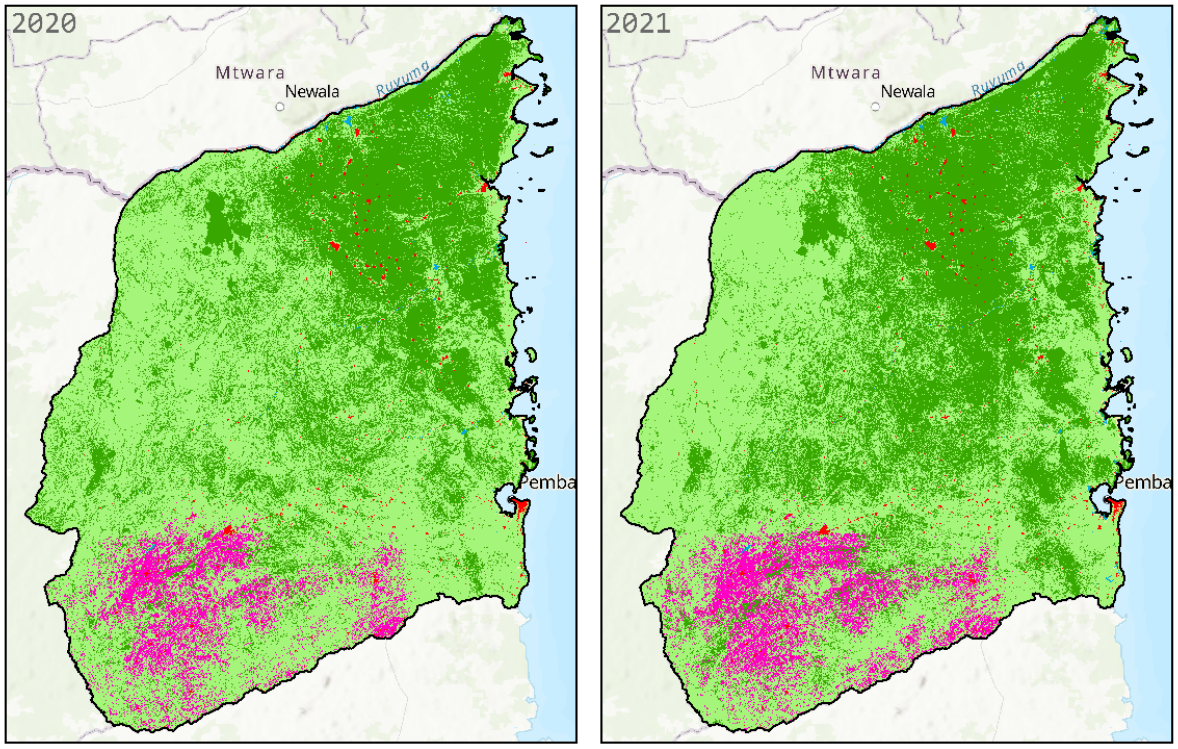

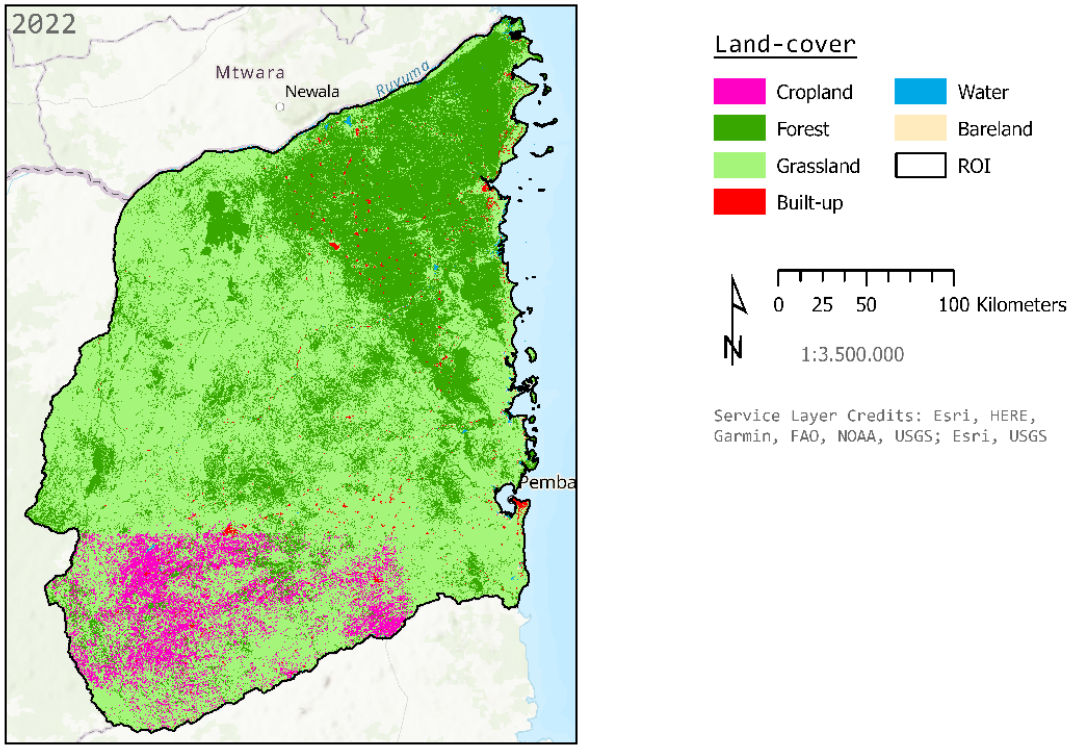

Figure 11: Annual land-cover maps for 2020, 2021, and 2022

The annual land-cover maps reached overall accuracies of 0.63 for 2020, 0.65 for 2021 and 0.58 for 2022, all +/- 0.04 with a confidence level of 95% (see Figure 12). Generally, the classes water and built-up were the most successful to classify with accuracies between 0.78 and 1.00. Cropland and bareland were the hardest to classify and show very low values in producer's accuracy (between 0.20 for cropland in 2021 and 2022 and 0.26 for bareland in 2021) which means that only around 20% of the reference crop and bare points have been correctly identified as crops or bareland. The calculated user's accuracy is the lowest for the class grassland (around 0.30 each year) meaning that only around 30% of the areas identified as grassland in the classification were actually grassland. Forest (2020: 102, 2021: 85, 2022: 129), cropland (2020: 61, 2021: 74, 2022: 66) and bareland (2020: 23, 2021: 26, 2022: 21) reference points were mistakenly classified as grassland (see Figure 12).

F1-scores for cropland were especially low with values between 0.32 +/- 0.03 (2021) and 0.37 +/- 0.04 (2020), with a confidence level of 95% (see Figure 12). While the classes grassland and bareland also showed low F1-scores between 0.36 and 0.48, the other classes reached higher F1-scores between 0.67 (forest in 2022) and 0.99 (water bodies every year), indicating that the classification model was both able to identify classes correctly (PA), and accurate with the classes it did identify (UA).

2020		Actual class							UA
		Cropland	Forest	Grassland	Built-up	Water bodies	Bareland	**Sum**	
Predicted class	Cropland	33	3	0	0	0	0	**36**	0.92
	Forest	48	213	8	0	0	1	**270**	0.79
	Grassland	61	102	85	0	0	23	**271**	0.31
	Built-up	0	0	0	50	0	10	**60**	0.83
	Water bodies	0	0	0	0	50	1	**51**	0.98
	Bareland	0	0	0	0	0	11	**11**	1.00
	Sum	**142**	**318**	**93**	**50**	**50**	**46**	**699**	
	PA	0.23	0.67	0.91	1	1	0.24		**0.63**
	F-1 Score	0.37	0.72	0.47	0.91	0.99	0.39		
	95% confidence	0.04	0.03	0.04	0.02	0.01	0.04		

2021		Actual class							UA
		Cropland	Forest	Grassland	Built-up	Water bodies	Bareland	**Sum**	
Predicted class	Cropland	28	5	0	0	0	0	**33**	0.85
	Forest	40	228	6	1	0	1	**276**	0.83
	Grassland	74	85	87	1	0	26	**273**	0.32
	Built-up	0	0	0	48	0	6	**54**	0.89
	Water bodies	0	0	0	0	50	1	**51**	0.98
	Bareland	0	0	0	0	0	12	**12**	1.00
	Sum	**142**	**318**	**93**	**50**	**50**	**46**	**699**	
	PA	0.20	0.72	0.94	0.96	1	0.26		**0.65**
	F-1 Score	0.32	0.77	0.48	0.92	0.99	0.41		
	95% confidence	0.03	0.03	0.04	0.02	0.01	0.04		

2022		Actual class							
		Cropland	Forest	Grassland	Built-up	Water bodies	Bareland	**Sum**	UA
Predicted class	Cropland	29	3	0	2	0	0	**34**	0.85
	Forest	47	186	6	0	0	2	**241**	0.77
	Grassland	66	129	87	3	1	21	**307**	0.28
	Built-up	0	0	0	45	0	13	**58**	0.78
	Water bodies	0	0	0	0	49	0	**49**	1.00
	Bareland	0	0	0	0	0	10	**10**	1.00
	Sum	**142**	**318**	**93**	**50**	**50**	**46**	**699**	
	PA	0.20	0.58	0.94	0.9	0.98	0.22		**0.58**
	F-1 Score	0.33	0.67	0.44	0.83	0.99	0.36		
	95% confidence	0.03	0.03	0.04	0.03	0.01	0.04		

Figure 12: Confusion matrices for 2020, 2021, and 2022

Taking a closer look at the underlying satellite data as well as, for reasons of comparison, at PlanetScope mosaics in two exemplary areas in Cabo Delgado reveals that many agricultural fields have not been detected by the classification (see Figure 13). The figure shows the PlanetScope mosaic, a Sentinel-2 RGB composite, both for the month of August, and the result of the classification, each for three consecutive years (2020, 2021, 2022) and for two different areas in Cabo Delgado. The month of August has been chosen since this is a month after the harvest, which usually happens in May to June, and before the start of a new agricultural season. The two areas that are zoomed in are patches of approximately 8 km^2 and located in areas where agricultural fields are clearly noticeable as geometric rectangular fields on satellite imagery. One is located in the northern part of Cabo Delgado where no agriculture has been detected, just north of the town of Muidumbe. The other one is further south where the classification detected agriculture, north of the town of Balama (see Figure B1).

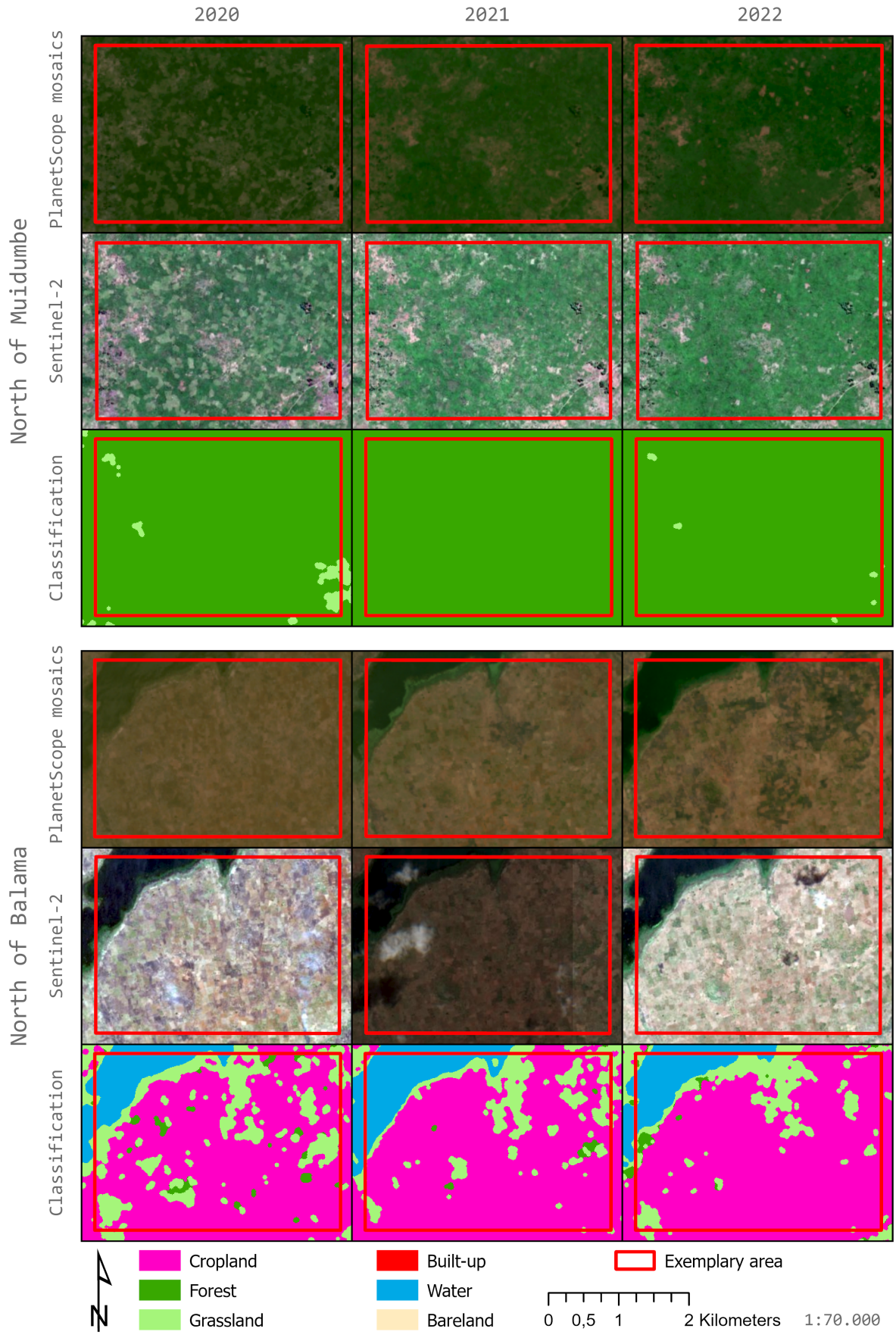

Figure 13: PlanetScope mosaic, Sentinel-2 imagery for August, and classification results for 2020, 2021, and 2022

Noticeable is, to begin with, that the classification did not detect agriculture correctly, in either example. Even though cropland is detected in the southern example (Balama), the detection seems random, not following any topographical features that are visible on the satellite images. Grassland and forest patches have been classified, but are not observable to the same extent on the imagery. For the northern example, the model only detected forest with some small grassland pixels. Furthermore, especially in example 1 which is located north of Muidumbe, in 2020 rectangular patterns typical for agricultural fields are visible, while in 2021 and 2022, these fields are not observable any more. This might be a sign of cropland abandonment, especially since the area has been severely affected by the conflict between 2019 and 2023 with 2020 being the most critical year in terms of number of events and fatalities (see Figure 14).

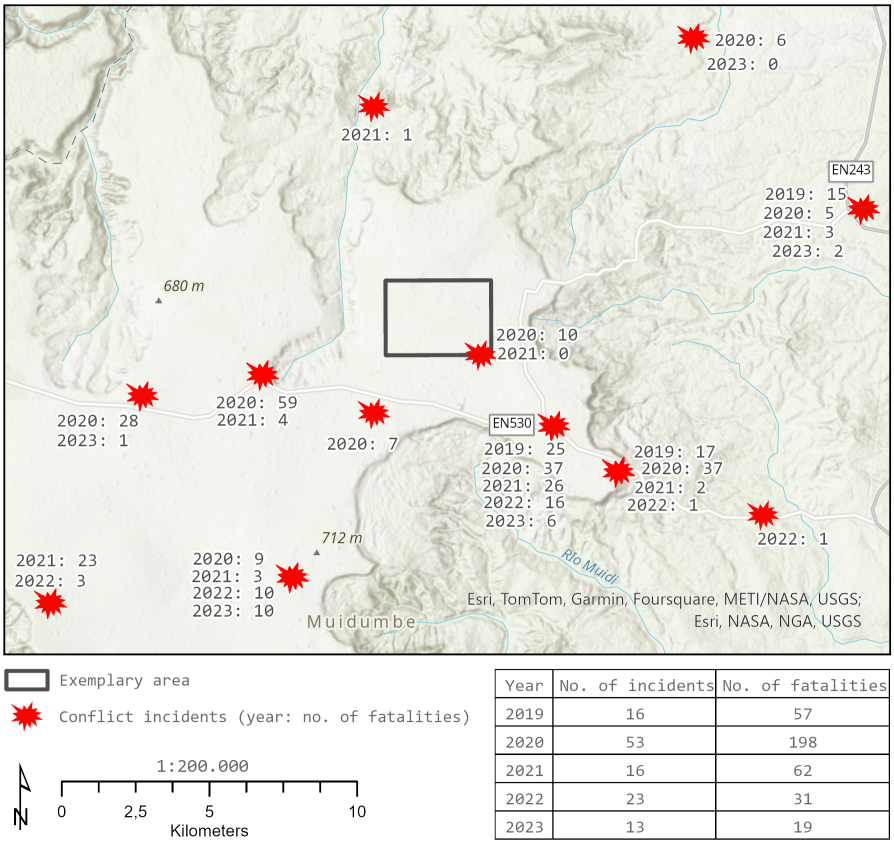

Year	No. of incidents	No. of fatalities
2019	16	57
2020	53	198
2021	16	62
2022	23	31
2023	13	19

Figure 14: Exemplary area north of Muidumbe with violent incidents

3.2 Annual Cropland Change

Bearing the classification results in mind, the validity of maps showing bi-temporal change has to be evaluated carefully. Since the purpose of this study is to analyse the abandonment of cropland, the class cropland is in focus in this section. Regarding the change maps for the own classifications, it is not surprising to see change in cropland only in the south-western part of Cabo Delgado (see Figure 15). Most changes are minor with a change of crop share below 20%, either positive or negative. Only in very few hexagon cells the change of crop share was higher than 50% (2020-2021: in 18 cells, 2021-2022: in 38 cells, out of 16,062 cells in total). Many cells show diverging directions in their change of cropland

share from one year to the other, for example having positive change from 2020 to 2021 and negative change from 2021 to 2022. While this can be related to an actual change of cropland resulting from population movement or crop rotation, it can also be a result of misclassifications and classification confusions between cropland and other classes.

The ESA change map shows a change in cropland all over the province. While many regions in the northern and south-western part of Cabo Delgado actually show a growth in cropland share from 2020 to 2021, the south-eastern districts seem to be losing cropland. However, again most changes are of low magnitude with a change of crop share less than +/- 20%. The changes are never more than +/- 50% (2.5km^2) per hexagon cell from 2020 to 2021.

The ESRI change maps interestingly show a reverse pattern from 2020/2021 to 2021/2022. While cropland share in many hexagons grew from 2020 to 2021, many of these exact same cells show a negative change from 2021 to 2022. This again might be due to actual cropland change but can also be a sign of misclassifications. The majority of changes is between -20% and +20%. Very few cells (387 of 16,062) have a change from 2020 to 2021 to 2022 in the same direction. Most of these show a loss of cropland.

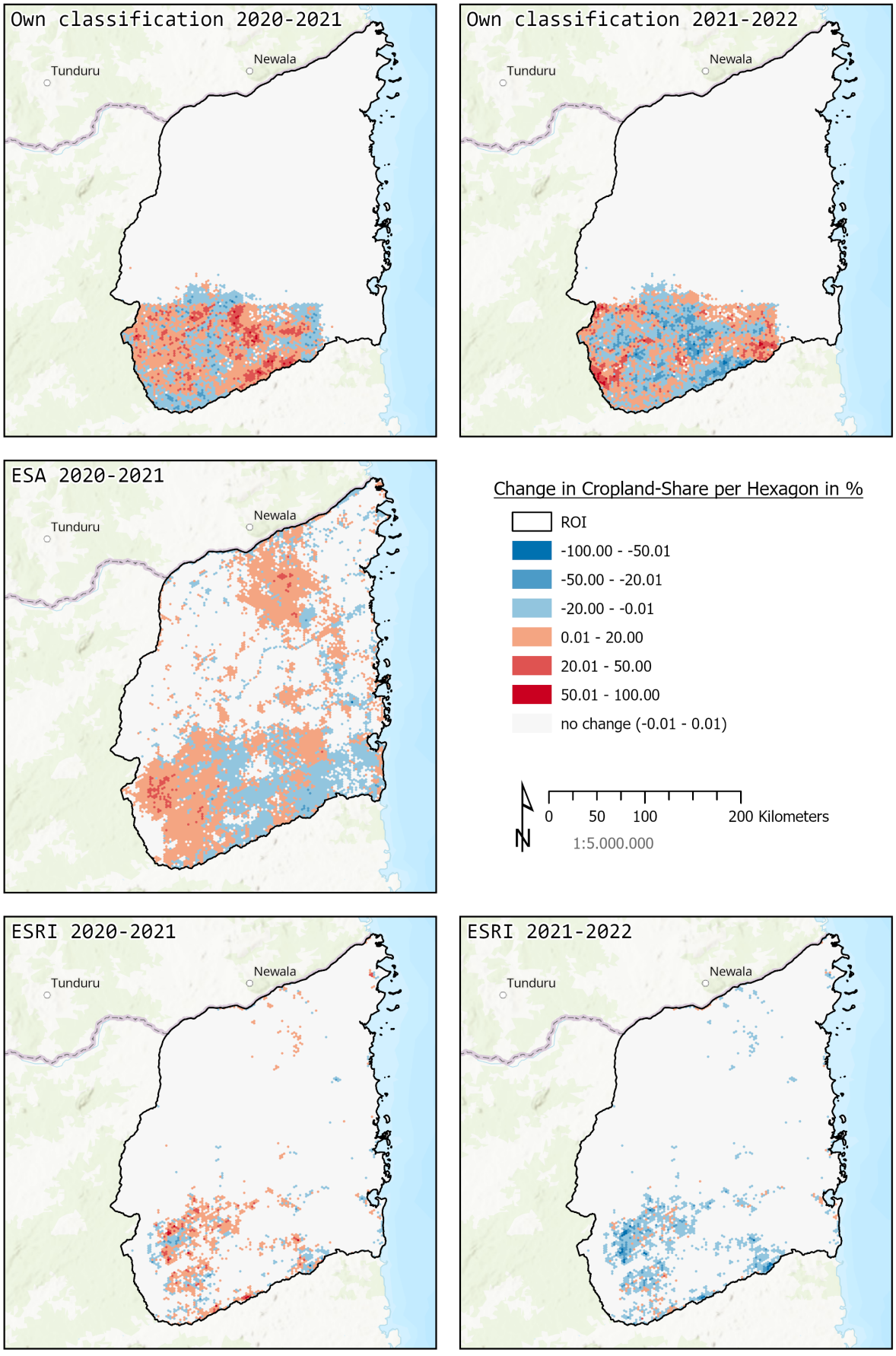

Figure 15: Cropland change in percent

3.3 Overlay with Conflict Data

As it can be seen in Figure 16, the conflict in Cabo Delgado started in the north and spread further south over the years, while still being mainly happening in the north-east. The maps display the relative density of conflict events, calculated using the feature count as the kernel density in a specific radius (here 25 screen unit points with a fixed scale of 1:2,500,000). It is important to bear in mind that these maps do not show the absolute number of events but rather the main locations where events took place. To clarify this, single dots are added to the maps, representing single incidents. However, these single conflict events overlap each other which is why a heat map offers a more appropriate visualization.

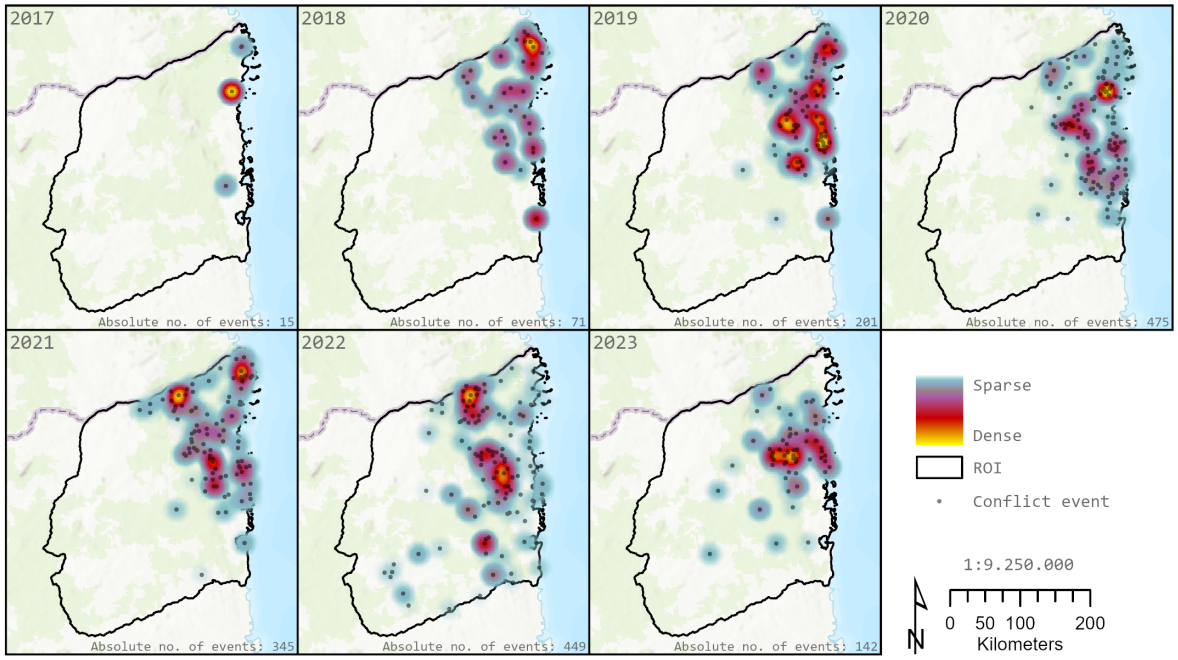

Figure 16: Relative density of conflict events in Cabo Delgado in 2017-2023

Since in this analysis a change in cropland was only detected in the south-western part of Cabo Delgado (see section 3.2), there does not seem to be a connection to the conflict that mostly took place in the north-east between 2020 and 2022. However, since the classification results show a low accuracy, the context between conflicts and cropland abandonment remains unclear.

Even with the ESA change map 2020-2021 as a benchmark, the pattern of cropland change does not seem to follow the spread of conflicts in 2020 and 2021 (see Figure C1).

However, as stated in section 3.1 and observable in Figures 13 and 14, visual signs of cropland abandonment that might be associated with violent incidents can be observed, although the link cannot be proven.

4 Discussion

This study presents an approach for detecting cropland abandonment in a conflict situation using Google Earth Engine and Sentinel-2 imagery. Unfortunately, the supervised classification has not worked well enough to detect the abandonment of agricultural fields. This is not only evident when looking at the confusion matrices (see Figure 12). Also a closer look at the satellite data underlying the analysis shows that many agricultural patches have not been recognized (see Figure 13). This is not uncommon in an area of the world like Cabo Delgado where subsistence and very small scale agriculture predominates. However, the analysis was based on a thorough literature review and was outlined according to general rules and best practices. In order to clarify why the results are not satisfying, a closer re-examination of the determining factors for the classification is needed. These include database, pre-processing, reference data generation, and RF model.

First, *database*: The aim of this study was to analyse the effects of a conflict on the change of cropland. The conflict in focus has already been ongoing for a few years, having started in 2017. With the purpose in mind of looking at a time-frame of several years, the selection of the underlying satellite data was done. Nowadays, there is a big selection of high quality satellite data freely available. One very interesting product is the PlanetScope mosaics with a resolution of 4.77m. These mosaics cover historical data from December 2015 to August 2020 with half-annual composites. From September 2020 to August 2022, these composites were updated monthly. Although this product is very interesting for analyses in the tropics, it was not chosen in this study since it could not provide a consistent database over the whole time-frame of the study, starting with monthly composites only in September 2020. With a different pre-processing approach, however, these mosaics could also have served as a valid database. They are already pre-processed and optimized for scientific and quantitative analysis, offering a ground-truth representation of spatially accurate data with minimized effects of atmosphere and sensor characteristics. They include four bands (R, G, B, NIR) which makes them suitable for a variety of vegetation indices. Some studies already explored their potential for mapping smallholder landscapes (e.g. Rufin et al., 2022). It is promising to repeat this study with PlanetScope mosaics.

The chosen product, still, is of high quality as well. A spectral comparison of both products (Sentinel-2 and PlanetScope mosaics) reveals their similarities (see Figures D1 to D4). The spectral profiles are based on the validation sample used in this study (699 points, see section 2.6). Their labels are reliable. For comparison reasons, only the Red, Green, Blue, and NIR bands are shown, since PlanetScope mosaics only hold these bands. The spectral profiles (Figures D1 and D2) demonstrate that the class differences over all classes except ‘water’ are relatively small. The class profiles have the same general shape and the average reflectance values are similar at each wavelength. Especially ‘cropland’ and ‘grassland’ are too close to expect good initial results for classification. From this, it would be advisable to re-create the training sample to capture the differences between the classes better. This can also be observed in the scatter plots in Figures D3 and D4. They represent the ratio of the NIR level to the Red level which is often used to identify vegetation. The three vegetation classes ‘forest’, ‘grassland’ and ‘cropland’ are indeed very close, while ‘water’, ‘built-up’ and ‘bareland’ show more distinct ratios. However, while

showing the need to re-adjust the training sample (which is only used here for demonstration purposes), the spectral comparison between Sentinel-2 and PlanetScope mosaics reveals that both products should be good datasets to be used in a supervised classification.

The availability of data with the same quality level influenced the decision of both, database and time-frame of the study: The chosen Sentinel-2 satellite images are openly available on Level 2A, which is atmospherically corrected, from January 2019 onwards. While the first outline of this study was to also look at satellite data from the time right before the conflict's outbreak in 2017, having a consistency in the database was chosen to be more important and therefore, the time-frame of the study was adjusted to the availability of Sentinel-2 data on Level 2A. Hence, the database was of high quality and consistency. However, in a pixel-based classification, mixed pixels covering more than one land-cover class can be problematic for the model. For this reason, especially in a highly fragmented smallholder landscape like Cabo Delgado's, small spatial resolutions are preferable.

As expected, the cloud cover for the wet seasons was extremely high. Only about 30% of the available images were taken into consideration, all images with a cloud cover of more than 30% were filtered out (see Figure 6). However, the pre-processing and compositing filled gaps satisfactory and made sure to have enough observations per pixel. A rough estimation with Google Earth Engine revealed a minimum of 6 observations per pixel location and a mean value of 18 each year (it has to be noted that the observations on overlapping paths are counted twice, hence the actual mean value is lower).

The *pre-processing* steps included cloud and shadow masking, gap filling, indices calculation, seasonal aggregation, percentile and texture calculation. While cloud and shadow masking and gap filling cleared and smoothed the database, indices, percentiles and texture added additional information to enhance the identification of different land-cover classes. Cloud filtering reduced the number of images substantially, especially in the wet season from November to May. For the wet season 2019/2020 for example, 588 images (63%) had a cloud cover of more than 30% and were filtered out (see Figure 6). The step of seasonal aggregation reduced the database further, especially in regard to the temporal dimension. Out of between 344 and 501 single images (see Figure 6), one seasonal composite was created, reducing the temporal dimension from 344-501 data points to only one point in time. With the calculation of percentiles, this reduction is taken into account, representing the spread of data points over the time period. Nevertheless, the seasonal aggregation might be reducing the line of data points to a point where useful information is neglected. A different seasonal aggregation might return better results. Rufin et al. (2022) for example calculated metrics for three seasons ranging from September through December, January through April, and May through August following Bey et al. (2020).

The probably most critical issue for the success of a supervised classification like the one here, is the process of generating *training data*. In order to quickly generate a training dataset, the approach chosen here used existing land-cover datasets and reduced the areas from which training data was taken to only those pixels that were classified as the same land-cover in all datasets. First, class definitions may vary between datasets resulting in factual different classes, even if they are named equally. This can contaminate the training dataset taken out of the 'full agreement areas'. Second, the validity of the

training data is directly related to the validity of the underlying land-cover maps. Figure E1 summarizes the overall, user's and producer's accuracies by land-cover class for the used land-cover datasets. The accuracies of these maps vary widely and show less accurate classifications in areas like Cabo Delgado with small subsistence agriculture. While these accuracies have to be regarded with care since they were obtained on different scales (e.g. ESA on a continental scale, providing accuracies for Africa, and ESRI and FROM-GLC on a global scale), it is noticeable that the, for this study, likewise most relevant and most confused classes cropland and grassland are those with the highest variance in their accuracy. Also, since a chain is only as strong as its weakest link, only one mistakenly classified pixel in one of the underlying maps can produce follow-up confusions. By including a number of datasets and thereby ruling presumably wrong classifications out, however, this problem is taken into account, but is certainly not completely eliminated. Moreover, the approach produces another problem that this study clearly demonstrates: it reduces the reference database to a point where the model makes erroneous assumptions which in this case were also connected to location.

Specifically, the agricultural areas consistent over all datasets were located in Cabo Delgado's south-west - therefore most of the training points for cropland were put there, too (see Figure 17). Together with the auxiliary data of latitude and longitude, this local concentration probably caused false modelling by overestimating the correlation between spatial location and land-cover. This was proved by repeating the classification with a different training set. For a quick and simple assessment, again, the known validation dataset (699 points, see section 2.6) was used for that, expecting it to be of highest consistency and quality. Because of its size and class distribution, it is still not the most suitable training dataset for the given task, however, it provides a quick review regarding the assumed errors within the original training dataset. The validation dataset was partitioned into 70% training (490) and 30% evaluation points (209). No other input variables for the model were changed. Even though no further model improvement has been made, the classifications using this reference dataset reached already overall accuracies of 79% (2020), 80% (2021), and 76% (2022) with user's and producer's accuracies between 66% and 85% and the F1-score between 0.72 and 0.78 for the class cropland (see Figure F2). The classification of grassland was the least accurate, underscoring the difficulties associated with classifying this type of land-cover. The classified maps reflect a complete different land-cover pattern with forest being the predominant land-cover class and cropland being spread all over the province (see Figure F1).

It can be concluded that the technique of overlaying existing datasets to generate training data can only work well under certain conditions:

- First, the class definitions of all used datasets need to be consistent, making sure that no mixed classes are present.
- Second, the existing land-cover maps have to reach highest accuracies, also locally.
- Third, the training data should be spread over the region of interest as much as possible if it can be assumed that each land-cover class is spread over the region as well.
- Finally, it should be taken into consideration to have the obtained training points or polygons further reviewed by experts to make sure that their class assignment is correct.

Omission errors for cropland were forest and grassland while commission errors of cropland were negligible. Forest, grassland and cropland were the most confused classes resulting in the lowest accuracies. However, the interpretation of the confusion matrix only makes sense if also the validation sample is of high quality and allows an independent evaluation of the classification. The validation data used here was taken out of a separate study (Rufin et al., 2022) and was modified to adjust it to the needs of the current analysis. Figure 17 shows the distribution of validation points and their assigned classes in Cabo Delgado. They are more spread over the province than the training points which represents the reality more appropriately. They are also located in a suitable distance to the training points, ensuring their independence. Hence, the quality and size of the validation dataset used in this study is adequate and reasonable.

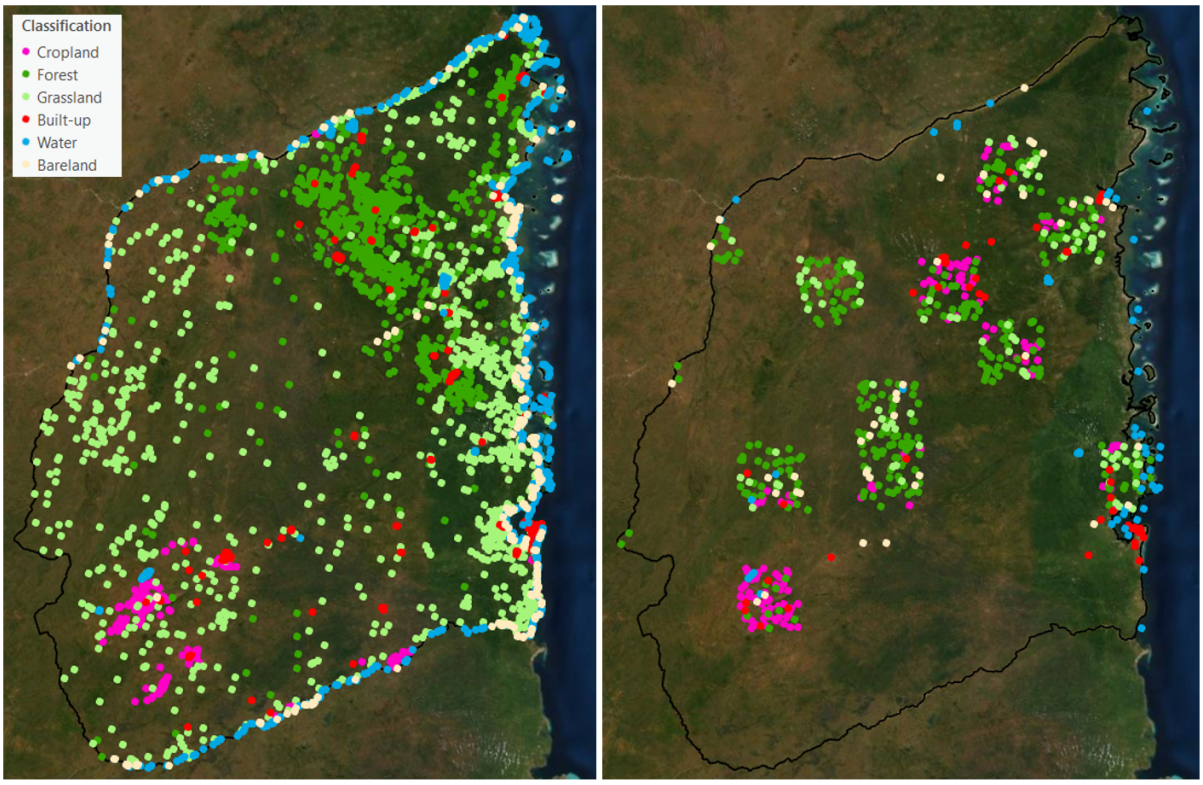

Figure 17: Training- (left) and validationpoints (right) and their assigned classes

The *RF classification* process in Google Earth Engine worked well and fast. Feature importance has been calculated in GEE where the importance is a measure of the decrease of Gini impurity. For each variable, the sum of the Gini decrease across every tree of the forest is accumulated every time that variable is chosen to split a node. The sum is divided by the number of trees in the forest to give an average. Each year, latitude and longitude reached the highest importance together with elevation (see Figure 18). This is unexpected and not easy to explain. It might be due to the speciality that lie in latitude and longitude data. While they are represented as floats, they are more similar to categorical or nominal data. A decrease or increase in magnitude does not give meaningful insights to the model. It would be interesting to see if the classification would be more accurate without geographic location or with distance metrics instead that are derived from coordinates. Also of high importance each year

were the texture measures 'sum average' (measures the sum of the averages of all grey levels) in all three kernel sizes as well as 'dissimilarity' and 'contrast' in kernel size 20, also the 25th percentile of GCVI for the dry season. Apparently, texture is an important feature, together with vegetation indices which were of higher importance than most of the spectral bands alone (see Figure 18). The figure shows the relative importance of features for the RF classification. The unit and scale, that differ from year to year, are irrelevant.

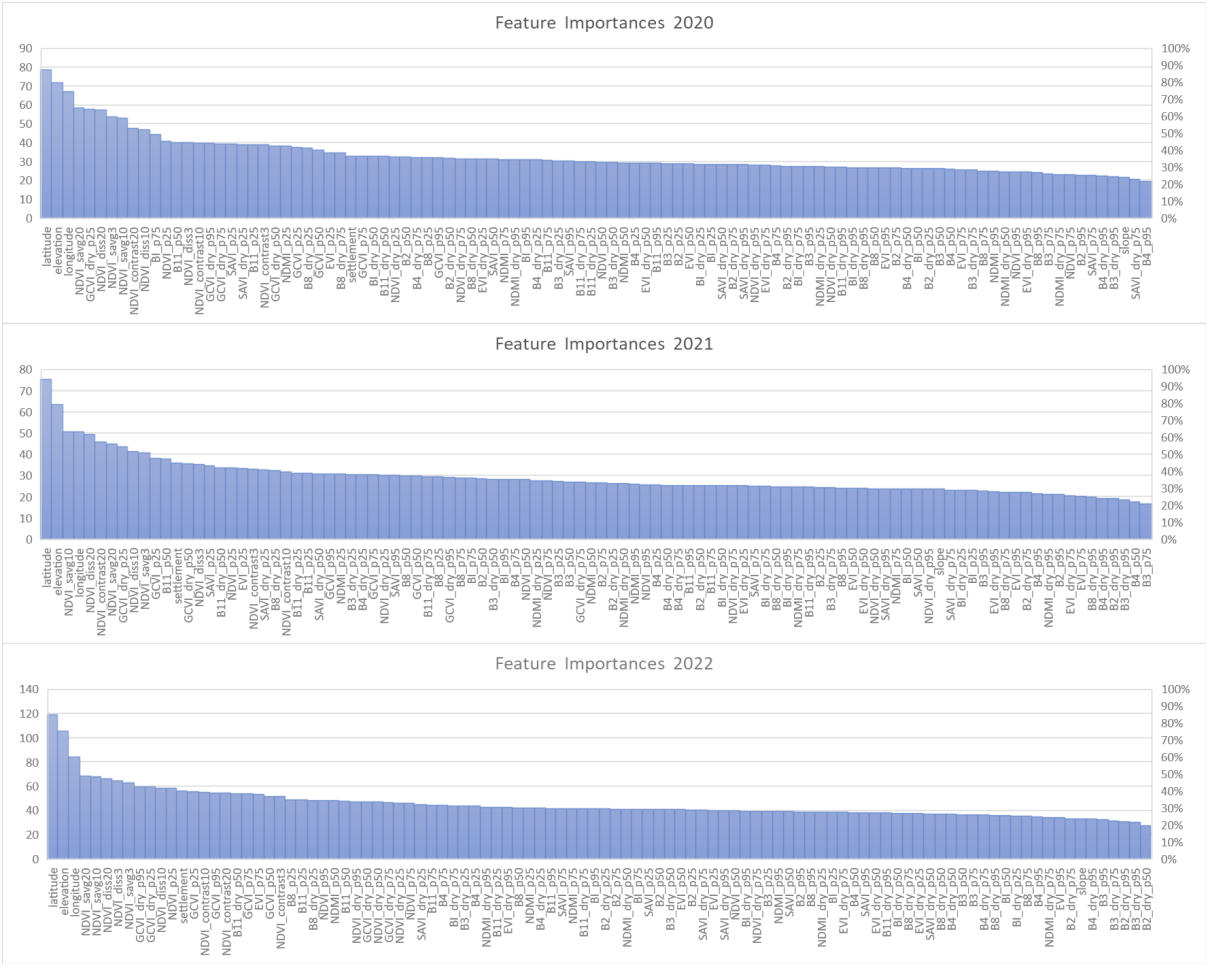

Figure 18: Feature importances for classifications 2020, 2021, and 2022

Other successful studies in cropland detection combined object-based and pixel-based classification approaches and included additional RS data like radar (e.g. J. Xiong et al., 2017; Yin et al., 2018). Given the usually geometric rectangular fields in agriculture (see Figure 13), these are paths that are worth to follow in order to improve classification results in areas like Cabo Delgado.

This master thesis defined abandoned cropland as agricultural fields that were not detected as agricultural fields in the following year. This definition is very narrow and might involve fallow fields that are not ploughed as part of the crop cycle. However, since the study tried to analyse quickly changing patterns in a conflict situation, the definition is appropriate here. Likewise, the detection of changes using a pixel-based post-classification approach is known to be valid. With a more accurate classification, the chosen approach could have reached meaningful insights.

5 Conclusions

Mozambique is an "invisible emergency" (UNHCR, 2022). This master thesis tried to make indicators of that emergency visible. Because of conflicts and natural disasters, Cabo Delgado's population is on the move and facts about the situation on-site are hard to get. The analysis of remotely sensed data can bring clarity into this critical situation. Powerful applications and the availability of an immense abundance of data seem to be simplifying the task. However, the process is complex and many aspects need to be taken into account.

The analysis launched with a broad literature review that revealed that there are many approaches to find answers to the following questions:

- Is cropland getting abandoned in Cabo Delgado?
- Is cropland predominantly abandoned in areas close to conflict events with violence against civilians?
- And can cropland abandonment thereby be an indicator of population displacement?

Regarding the first question: Since the automated approach using a supervised classification and a bi-temporal change analysis did not securely reveal an abandonment of cropland, a visual comparison is needed. In exemplary areas, signs of abandonment of agricultural fields can be seen (see Figure 13) that could probably also have been revealed by a better working automated detection approach.

Secondly, might this abandonment be due to the current conflict situation? Conflict events that happened in the vicinity of these presumably fallow fields might be the reason for abandonment. However, this connection can neither be clearly determined and needs further investigation, for example in the form of a propensity score matching analysis (Olsen et al., 2021) or regression models to explain agricultural land abandonment (Yin et al., 2019).

Finally, since neither cropland abandonment nor its connection to violent incidents in Cabo Delgado could have been detected with certainty, the last question concerning the indication of population displacement has not been further touched here. It is suggested to explore this further, for example by including and analysing data from the International Organization of Migration (IOM) which conducts and supports data production and research about migration patterns and processes. Data is regularly published on the organization's website (www.iom.int).

In summary, the approach chosen here did unfortunately not answer the research questions satisfyingly. Cropland abandonment could not be found as an indicator of population displacement. Furthermore, it could not clearly be detected and/or connected to the conflict in Cabo Delgado.

In a conflict situation, quick information is needed to organize humanitarian aid as fast as possible. Therefore, a classification based on yearly composites and employing a post-classification change detection approach to detect abandoned fields might not be the most efficient. In other studies that reached higher accuracies in classifying active cropland (e.g. Estel et al., 2015; Rufin et al., 2022), fallow fields and active cropland were classified as separate classes, making a subsequent change detection superflu-

ous. Presumably, such an automated and direct classification of fallow or abandoned fields might be more appropriate for quick responses when humanitarian aid is needed.

EPILOGUE

As a beginner in the field of remote sensing and with Google Earth Engine, I learned a ton in the course of this master thesis! Just for that, it was worth the effort, even if the results did not meet my hopes and expectations. As Neil Armstrong once said: “Research is creating new knowledge.” I would probably choose a different approach now with all the knowledge I have gathered. But one goal has been achieved: knowledge has been created!

The Google Earth Engine codes that were used for classification are made available at https://github.com/MerGeo33/GEE_codes.git.

REFERENCES

ACAPS. (2022). Mozambique Tropical Cyclones Season. In *ACAPS*. https://www.acaps.org/country/mozambique/crisis/tropical-cyclones-season.

ACAPS. (2023). *Mozambique: Impact of the five-year conflict in Cabo Delgado* (p. 8). ACAPS.

ACLED. (2023). ACLED Dashboard. In *ACLED*. https://acleddata.com/dashboard/.

Basnet, B. & Vodacek, A. (2015). Tracking Land Use/Land Cover Dynamics in Cloud Prone Areas Using Moderate Resolution Satellite Data: A Case Study in Central Africa. *Remote Sensing*, *7*(6), 6683–6709. https://doi.org/10.3390/rs70606683

Bey, A., Jetimane, J., Lisboa, S. N., Ribeiro, N., Sitoe, A. & Meyfroidt, P. (2020). Mapping smallholder and large-scale cropland dynamics with a flexible classification system and pixel-based composites in an emerging frontier of Mozambique. *Remote Sensing of Environment*, *239*, 111611. https://doi.org/10.1016/j.rse.2019.111611

Bofana, J., Zhang, M., Nabil, M., Wu, B., Tian, F., Liu, W., Zeng, H., Zhang, N., Nangombe, S., Cipriano, S., Phiri, E., Mushore, T. D., Kaluba, P., Mashonjowa, E. & Moyo, C. (2020). Comparison of Different Cropland Classification Methods under Diversified Agroecological Conditions in the Zambezi River Basin. *Remote Sensing*, *12*, 1–23. https://doi.org/10.3390/rs12132096

Breiman, L. (2001). Random Forests. *Machine Learning*, *45*(1), 5–32. https://doi.org/10.1023/A:1010933404324

Brown, C. F., Brumby, S. P., Guzder-Williams, B., Birch, T., Hyde, S. B., Mazzariello, J., Czerwinski, W., Pasquarella, V. J., Haertel, R., Ilyushchenko, S., Schwehr, K., Weisse, M., Stolle, F., Hanson, C., Guinan, O., Moore, R. & Tait, A. M. (2022). Dynamic World, Near real-time global 10 m land use land cover mapping. *Scientific Data*, *9*(1), 251. https://doi.org/10.1038/s41597-022-01307-4

CEMS. (2020a). *EMSN-063: Crop change detection in conflict areas, Nigeria*.

CEMS. (2020b). *EMSN-083: Crop change detection in conflict areas, Nigeria, October 2020*.

CEMS. (2021). *EMSN-113: Crop change detection in conflict-affected areas of Nigeria, agricultural season 2021*.

CEMS. (2022). *EMSN-138: Crop change detection in conflict-affected areas of Nigeria, agricultural season 2022*.

Conners, R. W., Trivedi, M. M. & Harlow, C. A. (1984). Segmentation of a high-resolution urban scene using texture operators. *Computer Vision, Graphics, and Image Processing*, *25*(3), 273–310. https://doi.org/10.1016/0734-189X(84)90197-X

Eklund, L., Degerald, M., Brandt, M., Prishchepov, A. V. & Pilesjö, P. (2017). How conflict affects land use: Agricultural activity in areas seized by the Islamic State. *Environmental Research Letters*, *12*(5), 054004. https://doi.org/10.1088/1748-9326/aa673a

El-Hattab, M. M. (2016). Applying post classification change detection technique to monitor an Egyptian coastal zone (Abu Qir Bay). *The Egyptian Journal of Remote Sensing and Space Science*, *19*(1), 23–36. https://doi.org/10.1016/j.ejrs.2016.02.002

ESA. (n.d.-a). Sentinel-2 MSI Spectral Resolution. In *Sentinel Online*. https://copernicus.eu/user-guides/sentinel-2-msi/resolutions/spectral.

ESA. (n.d.-b). User Guides - Sentinel-2 MSI - Level-2 Processing - Sentinel Online. In *Sentinel Online*. https://copernicus.eu/user-guides/sentinel-2-msi/processing-levels/level-2.

ESA. (2017). *ESA CCI LAND COVER – S2 prototype Land Cover 20m map of Africa 2016*. https://2016africalandcover20m.esrin.esa.int/.

ESRI. (2021). *ESRI 2020 Land Cover - Overview*. https://www.arcgis.com/home/item.html?id=8214141-a576848f69f440c793144f6ce.

ESRI ArcGIS Living Atlas of the World. (2022). *Sentinel-2 10m Land Use/Land Cover Time Series*. https://www.arcgis.com/home/item.html?id=cfcb7609de5f478eb7666240902d4d3d.

Estel, S., Kuemmerle, T., Alcántara, C., Levers, C., Prishchepov, A. & Hostert, P. (2015). Mapping farmland abandonment and recultivation across Europe using MODIS NDVI time series. *Remote Sensing of Environment*, *163*, 312–325. https://doi.org/10.1016/j.rse.2015.03.028

Famine Early Warning Systems Network. (2013). *Mozambique - Seasonal Calendar*. https://fews.net/southern-africa/mozambique/seasonal-calendar/december-2013.

Gong, P., Liu, H., Zhang, M., Li, C., Wang, J., Huang, H., Clinton, N., Ji, L., Li, W., Bai, Y., Chen, B., Xu, B., Zhu, Z., Yuan, C., Ping Suen, H., Guo, J., Xu, N., Li, W., Zhao, Y., ... Song, L. (2019). Stable classification with limited sample: Transferring a 30-m resolution sample set collected in 2015 to mapping 10-m resolution global land cover in 2017. *Science Bulletin*, *64*(6), 370–373. https://doi.org/10.1016/j.scib.2019.03.002

Government of Cabo Delgado Province. (2017). *Cabo Delgado Provincial Government Portal*. https://www.cabodelgado.gov.mz/por.

Haralick, R. M., Shanmugam, K. & Dinstein, I. (1973). Textural Features for Image Classification. *IEEE Transactions on Systems, Man, and Cybernetics*, *SMC-3*(6), 610–621. https://doi.org/10.1109/TSMC.1973.4309314

HarvestChoice & Institute (IFPRI), I. F. P. R. (2016). *Agro-Ecological Zones for Africa South of the Sahara*. Harvard Dataverse. https://doi.org/10.7910/DVN/M7XIUB

Huete, A. R. (1988). A soil-adjusted vegetation index (SAVI). *Remote Sensing of Environment*, *25*(3), 295–309. https://doi.org/10.1016/0034-4257(88)90106-X

IFAD. (2023). Mozambique. In *IFAD*. https://www.ifad.org/en/web/operations/w/country/mozambique.

IIASA. (2019). *Accuracy assessment of 20 m land cover map of Africa*. IIASA.

IOM. (2022). *Northern Mozambique Crisis: Displacement Tracking Matrix - DTM Baseline Assessment Abridged Report Round 16*. The International Organization for Migration.

IOM. (2023). *Mozambique Mobility Tracking Assessment Report 19 (August 2023)*. The International Organization for Migration.

IPC. (2023). *Mozambique: Acute Food Insecurity Situation November 2022 - March 2023*. IPC - Integrated Food Security Phase Classification.

Jalal, R., Qiyamud Din Ikram, Fatima Mushtaq, Amit Ghosh, Josselin Gauny, Daniele Barelli, Doug Muchoney, Khalid Cassam, Marco Falcone & Matieu Henry. (2022). *A rapid geospatial analysis of Nampula and Cabo Delgado provinces in Mozambique*. Food and Agriculture Organization of the United Nations.

Karra, K., Kontgis, C., Statman-Weil, Z., Mazzariello, J. C., Mathis, M. & Brumby, S. P. (2021). Global land use / land cover with Sentinel 2 and deep learning. *2021 IEEE International Geoscience and Remote Sensing Symposium IGARSS*, 4704–4707. https://doi.org/10.1109/IGARSS47720.2021.9553499

Kerner, H., Tseng, G., Becker-Reshef, I., Nakalembe, C., Barker, B., Munshell, B., Paliyam, M. & Hosseini, M. (2020). *Rapid Response Crop Maps in Data Sparse Regions*. arXiv. https://doi.org/10.48550/arXiv.2006.16866

Lesiv, M., Fritz, S., McCallum, I., Tsendbazar, N.-E., Pekel, J.-F., Herold, M., Buchhorn, M., Smets, B. & Van De Kerchove, R. (2017). *Evaluation of ESA CCI prototype land cover map at 20m*. https://doi.org/10.13140/RG.2.2.12135.34728

Lesiv, M., Laso Bayas, J. C., See, L., Duerauer, M., Dahlia, D., Durando, N., Hazarika, R., Kumar Sahariah, P., Vakolyuk, M., Blyshchyk, V., Bilous, A., Perez-Hoyos, A., Gengler, S., Prestele, R., Bilous, S., Akhtar, I. ul H., Singha, K., Choudhury, S. B., Chetri, T., … Fritz, S. (2019). Estimating the global distribution of field size using crowdsourcing. *Global Change Biology*, *25*(1), 174–186. https://doi.org/10.1111/gcb.14492

Löw, F., Prishchepov, A. V., Waldner, F., Dubovyk, O., Akramkhanov, A., Biradar, C. & Lamers, J. P. A. (2018). Mapping Cropland Abandonment in the Aral Sea Basin with MODIS Time Series. *Remote Sensing*, *10*(2), 159. https://doi.org/10.3390/rs10020159

Lu, D., Mausel, P., Brondízio, E. & Moran, E. (2004). Change detection techniques. *International Journal of Remote Sensing*, *25*(12), 2365–2401. https://doi.org/10.1080/0143116031000139863

Marconcini, M., Metz-Marconcini, A., Üreyen, S., Palacios-Lopez, D., Hanke, W., Bachofer, F., Zeidler, J., Esch, T., Gorelick, N., Kakarla, A., Paganini, M. & Strano, E. (2020). Outlining where humans live, the World Settlement Footprint 2015. *Scientific Data*, *7*(1), 242. https://doi.org/10.1038/s41597-020-00580-5

Morell-Monzó, S., Estornell, J. & Sebastiá-Frasquet, M.-T. (2020). Comparison of Sentinel-2 and High-Resolution Imagery for Mapping Land Abandonment in Fragmented Areas. *Remote Sensing*, *12*(12), 2062. https://doi.org/10.3390/rs12122062

NASA JPL. (2020). *NASADEM Merged DEM Global 1 arc second V001*. NASA EOSDIS Land Processes DAAC. https://doi.org/10.5067/MEASURES/NASADEM/NASADEM_HGT.001

National Institute of Statistics. (2023). *National Institute of Statistics - INE*. https://www.ine.gov.mz/.

Neethling, T. (2021). Conflict Dynamics in Mozambique's Cabo Delgado Province. In *ACCORD*. https://www.accord.org.za/conflict-trends/conflict-dynamics-in-mozambiques-cabo-delgado-province/.

Olsen, V. M., Fensholt, R., Olofsson, P., Bonifacio, R., Butsic, V., Druce, D., Ray, D. & Prishchepov, A. V. (2021). The impact of conflict-driven cropland abandonment on food insecurity in South Sudan revealed using satellite remote sensing. *Nature Food*, *2*(12), 990–996. https://doi.org/10.1038/s43016-021-00417-3

Planet Labs Inc. (2023). *NICFI Data Program*. https://www.planet.com/nicfi/.

Raleigh, C., Kishi, R. & Linke, A. (2023). Political instability patterns are obscured by conflict dataset

scope conditions, sources, and coding choices. *Humanities and Social Sciences Communications*, *10*(1), 1–17. https://doi.org/10.1057/s41599-023-01559-4

Rufin, P., Bey, A., Picoli, M. & Meyfroidt, P. (2022). Large-area mapping of active cropland and short-term fallows in smallholder landscapes using PlanetScope data. *International Journal of Applied Earth Observation and Geoinformation*, *112*, 102937. https://doi.org/10.1016/j.jag.2022.102937

Rufin, P., Rabe, A., Nill, L. & Hostert, P. (2021). GEE TIMESERIES EXPLORER FOR QGIS – INSTANT ACCESS TO PETABYTES OF EARTH OBSERVATION DATA. *The International Archives of the Photogrammetry, Remote Sensing and Spatial Information Sciences*, *XLVI-4/W2-2021*, 155–158. https://doi.org/10.5194/isprs-archives-XLVI-4-W2-2021-155-2021

Samasse, K., Hanan, N. P., Anchang, J. Y. & Diallo, Y. (2020). A High-Resolution Cropland Map for the West African Sahel Based on High-Density Training Data, Google Earth Engine, and Locally Optimized Machine Learning. *Remote Sensing*, *12*(9), 1436. https://doi.org/10.3390/rs12091436

Tappan, G. G., Cushing, W. M., Cotillon, S. E., Mathis, M. L., Hutchinson, J. A., Herrmann, S. M. & Dalsted, K. J. (2016). *West Africa Land Use Land Cover Time Series*. U.S. Geological Survey. https://doi.org/10.5066/F73N21JF

Tong, X., Brandt, M., Hiernaux, P., Herrmann, S., Rasmussen, L. V., Rasmussen, K., Tian, F., Tagesson, T., Zhang, W. & Fensholt, R. (2020). The forgotten land use class: Mapping of fallow fields across the Sahel using Sentinel-2. *Remote Sensing of Environment*, *239*, 111598. https://doi.org/10.1016/j.rse.2019.111598

Tsendbazar, N., Li, L., Koopman, M., Carter, S., Herold, M., Georgieva, I. & Lesiv, M. (2021). *World-Cover Product Validation Report (D12-PVR)*.

UNHCR. (2022). *UNHCR Mozambique Fact Sheet, June 2022*.

WFP. (2020). *Satellite imagery in conflict-affected areas. How technology can support WFP emergency response. Case Study Mali*.

Xiong, J., Thenkabail, P. S., Tilton, J. C., Gumma, M. K., Teluguntla, P., Oliphant, A., Congalton, R. G., Yadav, K. & Gorelick, N. (2017). Nominal 30-m Cropland Extent Map of Continental Africa by Integrating Pixel-Based and Object-Based Algorithms Using Sentinel-2 and Landsat-8 Data on Google Earth Engine. *Remote Sensing*, *9*(10), 1065. https://doi.org/10.3390/rs9101065

Xiong, S., Baltezar, P., Crowley, M. A., Cecil, M., Crema, S. C., Baldwin, E., Cardille, J. A. & Estes, L. (2022). Probabilistic Tracking of Annual Cropland Changes over Large, Complex Agricultural Landscapes Using Google Earth Engine. *Remote Sensing*, *14*(19), 4896. https://doi.org/10.3390/rs14194896

Yin, H., Brandão, A., Buchner, J., Helmers, D., Iuliano, B. G., Kimambo, N. E., Lewińska, K. E., Razenkova, E., Rizayeva, A., Rogova, N., Spawn, S. A., Xie, Y. & Radeloff, V. C. (2020). Monitoring cropland abandonment with Landsat time series. *Remote Sensing of Environment*, *246*, 111873. https://doi.org/10.1016/j.rse.2020.111873

Yin, H., Butsic, V., Buchner, J., Kuemmerle, T., Prishchepov, A. V., Baumann, M., Bragina, E. V., Sayadyan, H. & Radeloff, V. C. (2019). Agricultural abandonment and re-cultivation during and after the Chechen Wars in the northern Caucasus. *Global Environmental Change*, *55*, 149–159.

https://doi.org/10.1016/j.gloenvcha.2019.01.005

Yin, H., Prishchepov, A. V., Kuemmerle, T., Bleyhl, B., Buchner, J. & Radeloff, V. C. (2018). Mapping agricultural land abandonment from spatial and temporal segmentation of Landsat time series. *Remote Sensing of Environment*, *210*, 12–24. https://doi.org/10.1016/j.rse.2018.02.050

Zanaga, D., Van De Kerchove, R., Daems, D., De Keersmaecker, W., Brockmann, C., Kirches, G., Wevers, J., Cartus, O., Santoro, M., Fritz, S., Lesiv, M., Herold, M., Tsendbazar, N.-E., Xu, P., Ramoino, F. & Arino, O. (2022). *ESA WorldCover 10 m 2021 V200*. Zenodo. https://doi.org/10.5281/zenodo.7254221

Zanaga, D., Van De Kerchove, R., De Keersmaecker, W., Souverijns, N., Brockmann, C., Quast, R., Wevers, J., Grosu, A., Paccini, A., Vergnaud, S., Cartus, O., Santoro, M., Fritz, S., Georgieva, I., Lesiv, M., Carter, S., Herold, M., Li, L., Tsendbazar, N.-E., ... Arino, O. (2021). *ESA WorldCover 10 m 2020 V100*. Zenodo. https://doi.org/10.5281/zenodo.5571936

Appendix A

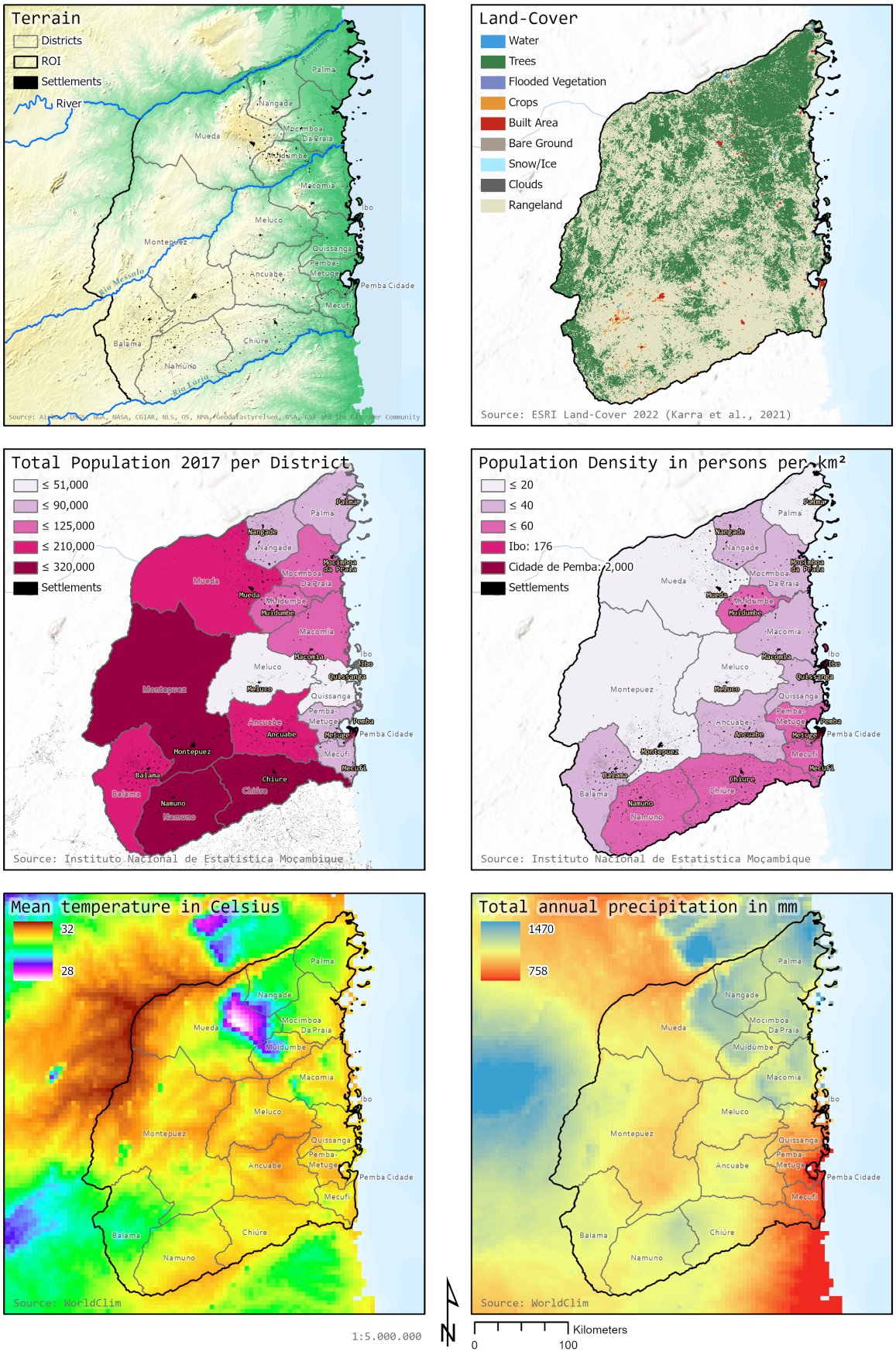

Figure A1: Cabo Delgado terrain, land-cover, population, temperature, and precipitation

Appendix B

Figure B1: Location of exemplary areas

Appendix C

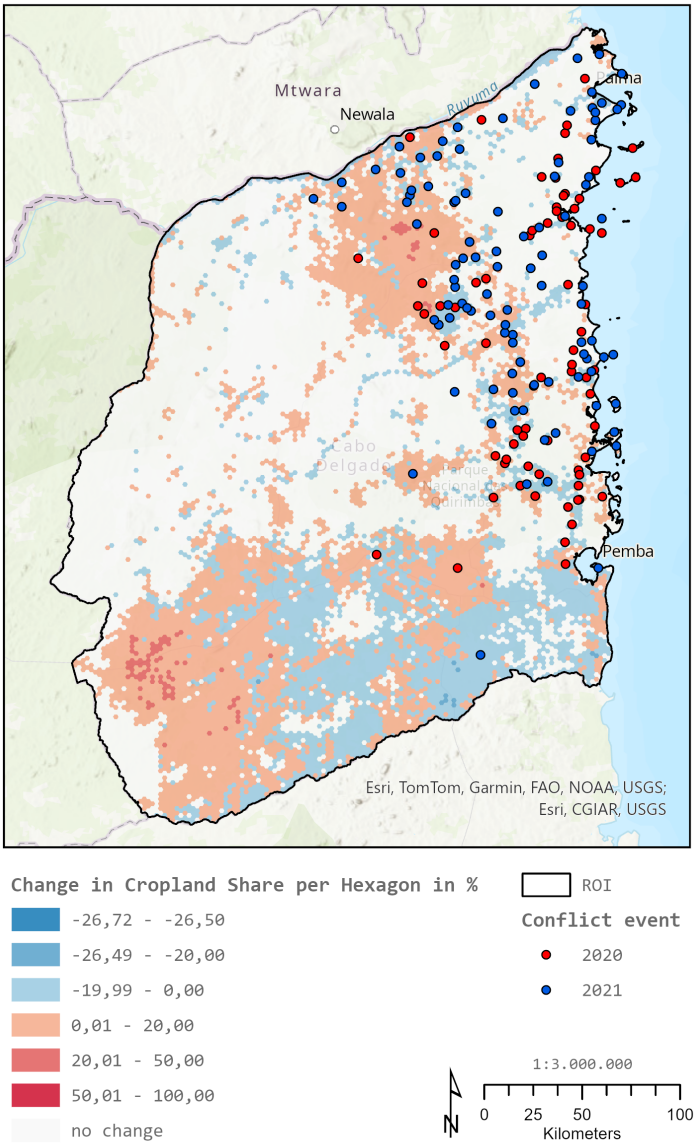

Figure C1: ESA cropland change 2020-2021 with conflict events 2020 and 2021

Appendix D

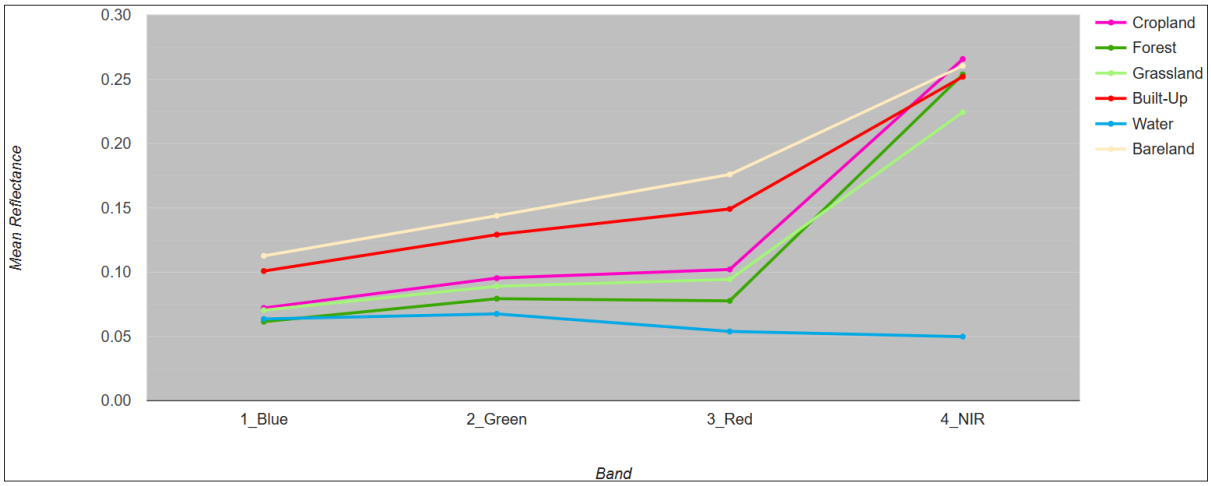

Figure D1: Sentinel-2 Surface Reflectance Spectra

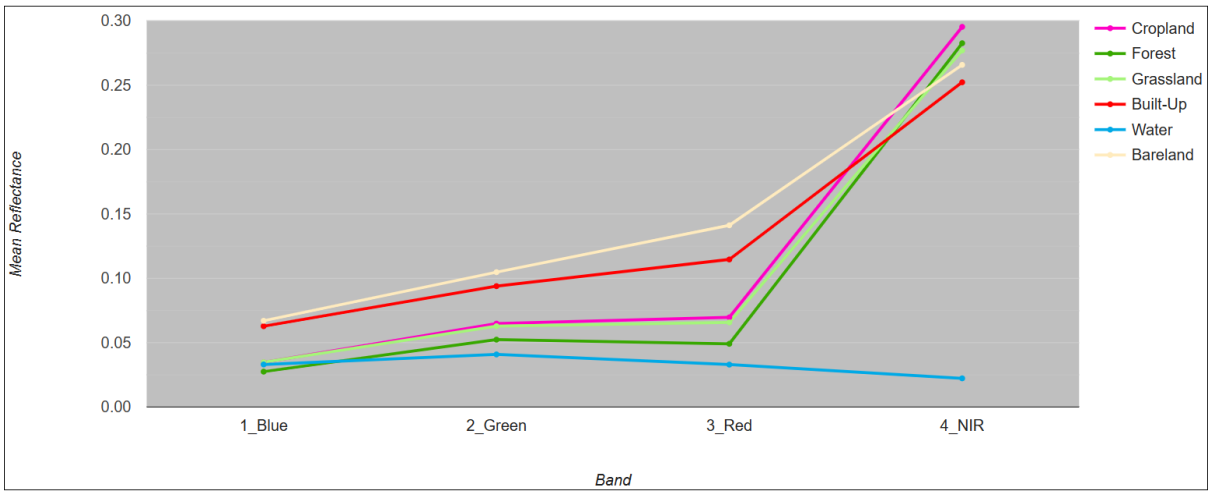

Figure D2: NICFI Surface Reflectance Spectra

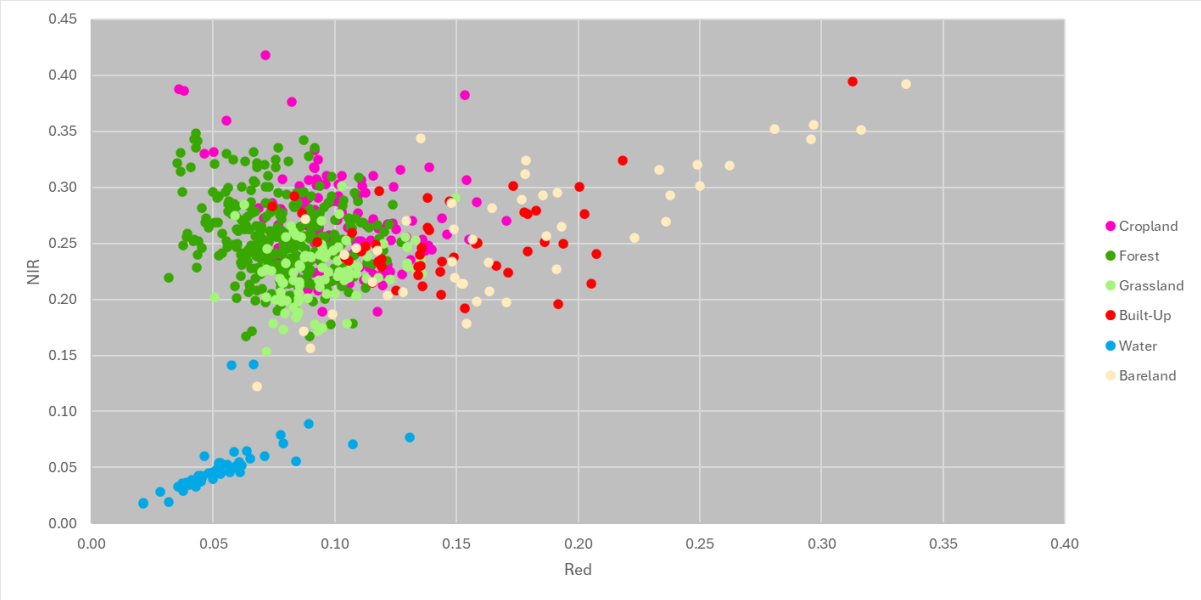

Figure D3: Sentinel-2 Scatter Plot NIR/Red

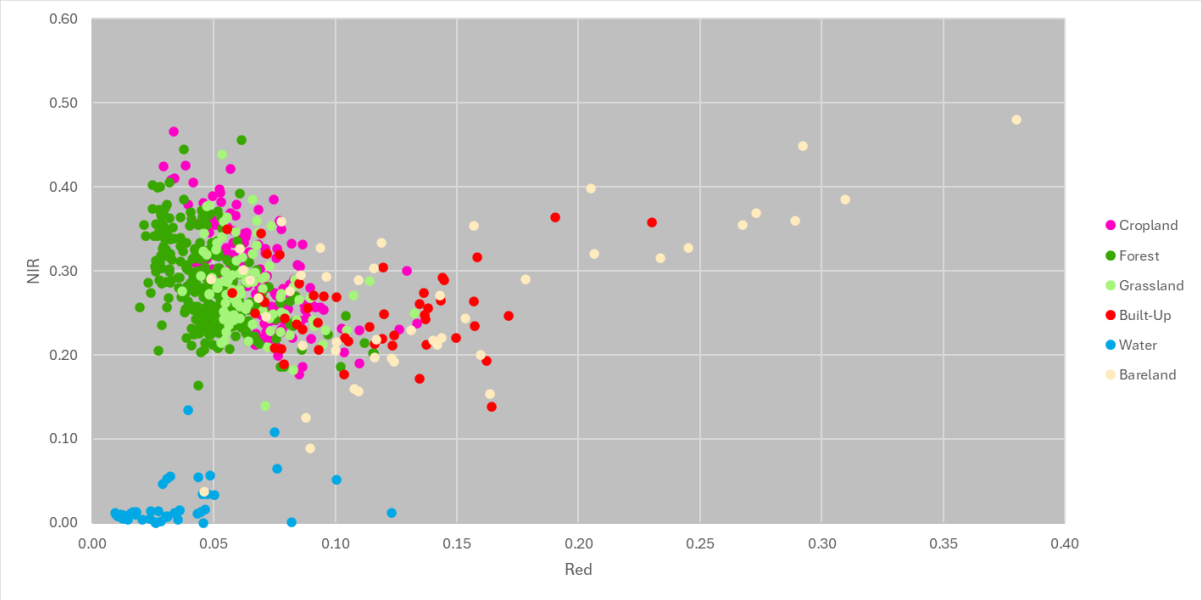

Figure D4: NICFI Scatter Plot NIR/Red

Appendix E

		ESA Worldcover 2020	ESRI Land-Cover 2020	FROM-GLC 2017	ESA CCI 2016
	Overall Accuracy	**73.63**	**85.96**	**72.76**	**64.30**
Cropland	UA	71.40	90.65	58.14	50.40
	PA	50.80	89.93	61.07	63.00
Forest	UA	62.33[1]	73.95[3]	73.11[4]	55.93[6]
	PA	73.53[1]	82.14[3]	67.49[4]	47.80[6]
Grassland	UA	64.65[2]	38.47	58.51	43.00
	PA	50.40[2]	47.20	64.49	34.90
Built-up	UA	45.50	95.79	61.76	67.30
	PA	71.10	83.69	72.19	17.90
Water	UA	90.60	82.99	89.18[5]	89.6
	PA	88.70	99.21	81.75[5]	32.5
Bareland	UA	94.40	61.36	81.40	83.50
	PA	91.10	87.40	84.58	93.60
	Source	Tsendbazar et al., 2021	ESRI, 2021	Gong et al., 2019	Lesiv et al., 2017
		[1] average of accuracies for tree cover, shrubland, and mangroves, [2] average of accuracies for grassland and herbaceous wetland	[3] average of accuracies for trees and flooded vegetation	[4] average of accuracies for forest and shrubland, [5] average of accuracies for water and snow/ice	[6] average of accuracies for trees, shrubs, and wetlands

Figure E1: Overall, user's and producer's accuracies in % by land-cover class

Appendix F

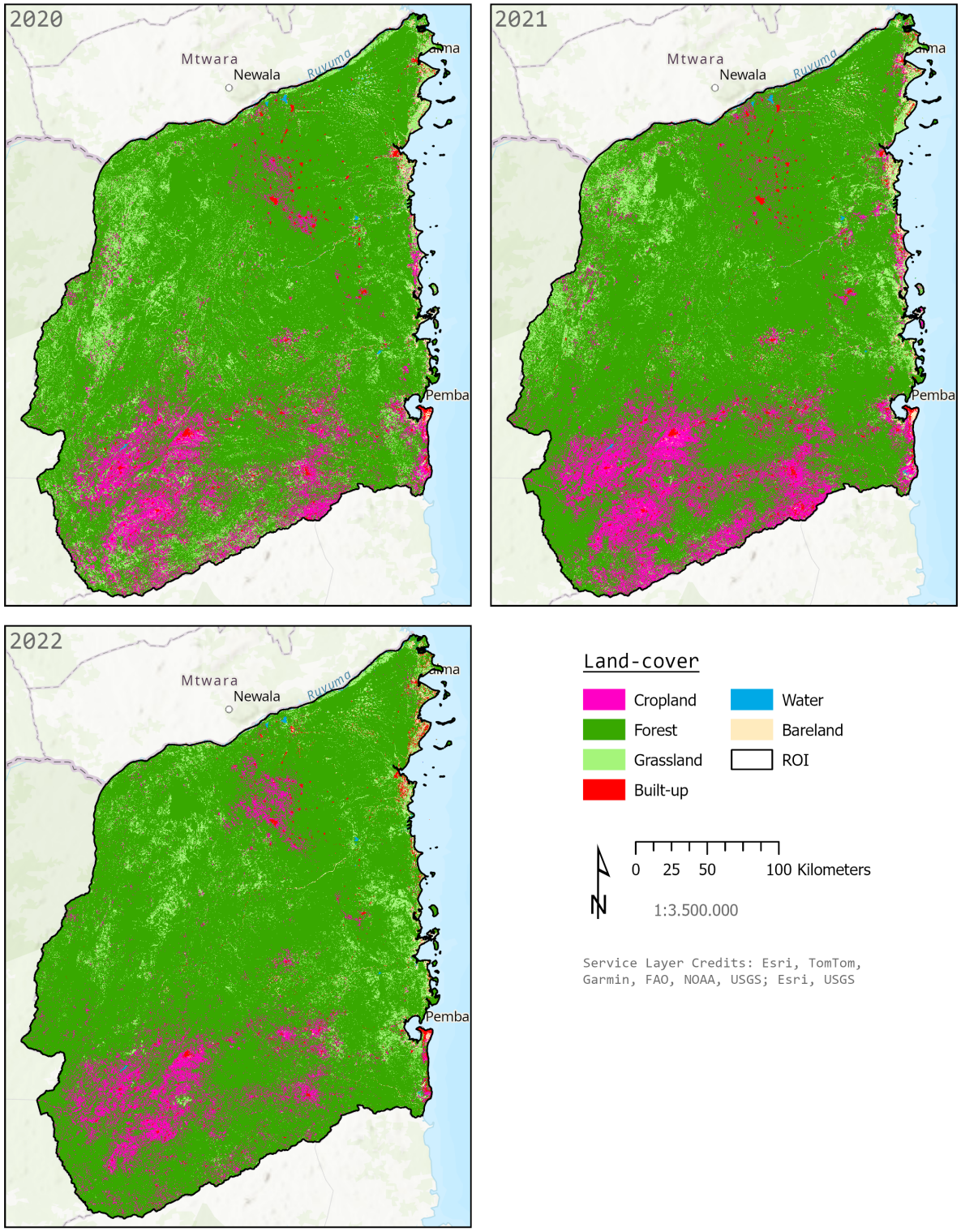

Figure F1: Classified maps with test dataset for 2020, 2021, and 2022

2020		Actual classes							
		Cropland	Forest	Grassland	Built-Up	Water	Bareland	**Sum**	UA
Predicted classes	Cropland	32	1	5	0	0	3	**41**	0.78
	Forest	12	81	10	0	0	1	**104**	0.78
	Grassland	2	3	11	0	1	2	**19**	0.58
	Built-Up	0	0	0	14	0	2	**16**	0.88
	Water	0	0	1	0	13	0	**14**	0.93
	Bareland	1	0	0	0	0	14	**15**	0.93
	Sum	**47**	**85**	**27**	**14**	**14**	**22**	**209**	
	PA	0.68	0.95	0.41	1.00	0.93	0.64		**0.79**
	F-1 Score	0.73	0.86	0.48	0.93	0.93	0.76		
	95% confidence	0.06	0.05	0.07	0.03	0.03	0.06		

2021		Actual classes							
		Cropland	Forest	Grassland	Built-Up	Water	Bareland	**Sum**	UA
Predicted classes	Cropland	34	3	1	0	0	2	**40**	0.85
	Forest	10	80	10	0	0	0	**100**	0.80
	Grassland	3	2	16	0	0	4	**25**	0.64
	Built-Up	0	0	0	12	1	4	**17**	0.71
	Water	0	0	0	0	13	0	**13**	1.00
	Bareland	0	0	0	2	0	12	**14**	0.86
	Sum	**47**	**85**	**27**	**14**	**14**	**22**	**209**	
	PA	0.72	0.94	0.59	0.86	0.93	0.55		**0.80**
	F-1 Score	0.78	0.86	0.62	0.77	0.96	0.67		
	95% confidence	0.06	0.05	0.07	0.06	0.03	0.06		

2022		Actual classes							
		Cropland	Forest	Grassland	Built-Up	Water	Bareland	**Sum**	UA
Predicted classes	Cropland	31	1	2	1	0	4	**39**	0.79
	Forest	14	80	13	0	0	0	**107**	0.75
	Grassland	2	4	11	2	0	4	**23**	0.48
	Built-Up	0	0	0	11	0	2	**13**	0.85
	Water	0	0	0	0	14	0	**14**	1.00
	Bareland	0	0	1	0	0	12	**13**	0.92
	Sum	**47**	**85**	**27**	**14**	**14**	**22**	**209**	
	PA	0.66	0.94	0.41	0.79	1.00	0.55		**0.76**
	F-1 Score	0.72	0.83	0.44	0.81	1.00	0.69		
	95% confidence	0.06	0.05	0.07	0.05	0.00	0.06		

Figure F2: Confusion matrices with test dataset for 2020, 2021, and 2022